

Electronic energy transfer through non-adiabatic vibrational-electronic resonance. II. 1D spectra for a dimer

Vivek Tiwari and David M. Jonas^{a)}
Department of Chemistry and Biochemistry, University of Colorado, 215 UCB, Boulder, Colorado 80309, USA
(Received 4 September 2017; accepted 25 January 2018; published online 26 February 2018; publisher error corrected 28 February 2018)

Vibrational-electronic resonance in photosynthetic pigment-protein complexes invalidates Förster's adiabatic framework for interpreting spectra and energy transfer, thus complicating determination of how the surrounding protein affects pigment properties. This paper considers the combined effects of vibrational-electronic resonance and inhomogeneous variations in the electronic excitation energies of pigments at different sites on absorption, emission, circular dichroism, and hole-burning spectra for a non-degenerate homodimer. The non-degenerate homodimer has identical pigments in different sites that generate differences in electronic energies, with parameters loosely based on bacteriochlorophyll a pigments in the Fenna-Matthews-Olson antenna protein. To explain the intensity borrowing, the excited state vibrational-electronic eigenvectors are discussed in terms of the vibrational basis localized on the individual pigments, as well as the correlated/anti-correlated vibrational basis delocalized over both pigments. Compared to those in the isolated pigment, vibrational satellites for the correlated vibration have the same frequency and precisely a factor of 2 intensity reduction through vibrational delocalization in both absorption and emission. Vibrational satellites for anti-correlated vibrations have their relaxed emission intensity reduced by over a factor 2 through vibrational and excitonic delocalization. In absorption, anti-correlated vibrational satellites borrow excitonic intensity but can be broadened away by the combination of vibronic resonance and site inhomogeneity; in parallel, their vibronically resonant excitonic partners are also broadened away. These considerations are consistent with photosynthetic antenna hole-burning spectra, where sharp vibrational and excitonic satellites are absent. Vibrational-excitonic resonance barely alters the inhomogeneously broadened linear absorption, emission, and circular dichroism spectra from those for a purely electronic excitonic coupling model. Energy transfer can leave excess energy behind as vibration on the electronic ground state of the donor, allowing vibrational relaxation on the donor's ground electronic state to make energy transfer permanent by removing excess energy from the excited electronic state of the dimer. © 2018 Author(s). All article content, except where otherwise noted, is licensed under a Creative Commons Attribution (CC BY) license (http://creativecommons.org/licenses/by/4.0/). https://doi.org/10.1063/1.5003193

I. INTRODUCTION

The remarkable efficiency of photosynthetic light harvesting has been a mystery since the 1930s. Recently, Tiwari et al. argued that low temperature absorption spectra of a photosynthetic light harvesting antenna and the Raman spectra of the isolated pigments imply a vibrational-electronic resonance between singly excited electronic states of the antenna and showed that reported 2D spectroscopic signatures are consistent with such a resonance for a model dimer with one vibration per pigment.² For this model, the delocalized anti-correlated linear combination of intramolecular vibrations causes a breakdown of Förster's adiabatic framework³ for energy transfer. In Paper I,¹¹ starting from a Hamiltonian for a dimer embedded in a protein, a nonadiabatic energy gap "tuning coordinate" for energy transfer between pigments was formulated to generalize the antisymmetric homodimer vibration in theories³ of electronic energy

transfer. This paper uses that Hamiltonian to investigate the role of additional pigment and protein vibrations and how absorption, emission, circular dichroism, and hole-burning spectra are modified by vibrational-electronic resonance for parameters appropriate to chlorophylls in photosynthetic light harvesting antennas. The key questions to be answered are as follows: How are systematic vibrational-excitonic resonances consistent with the wide body of spectroscopic experiments on photosynthetic systems? How should the parameters controlling resonance be determined? This paper emphasizes how interpretation of 1D spectra are and are not distorted by the vibrational-excitonic resonances present in some photosynthetic antenna proteins. As in the pioneering investigations of photosynthetic electron transfer by Friesner and co-workers, 4–7 the results obtained here indicate that vibronic complications in spectra of the antenna are such that the spectra of the isolated monomers, in combination with the linear absorption and circular dichroism spectra of the antenna, provide sound initial estimates for the underlying parameters of a vibrational-excitonic resonance model for energy transfer.



a)Author to whom correspondence should be addressed: david.jonas@ colorado.edu.

Approximations from more strongly coupled systems assume that vibrational and electronic excitation stay together as a vibronic exciton during electronic energy transfer.⁸ For a dimer with one Franck-Condon (FC) active mode on each pigment, we briefly show that non-adiabatic energy transfer to the acceptor pigment also involves a pathway where after electronic "de-excitation," the donor pigment is still left vibrationally excited on its electronic ground state. The coherent exciton scattering (CES) approximation and the "one-particle" approximation of the vibronic-exciton model^{9,10} assume that vibrational and electronic excitation stick together and thus fail to capture this essential pathway. By contrast, pathways in which either the donor or acceptor can be left vibrationally excited are both simultaneously present for energy transfer that excites an anti-correlated vibration delocalized over both pigments. This doubles the non-adiabatic enhancement of vibrational amplitude on both the ground and excited states of the antenna as a whole. In the Golden rule rate equation limit, this additional pathway doubles the energy transfer rate.11

Non-adiabatic vibrational-electronic mixing has a finite width around the resonant vibrational frequency. The resonance width also makes it essential to consider additional resonant or near-resonant vibrations. Two kinds of effects involving more than one coupled intramolecular vibration are considered here. In one, a FC active vibrational is split into two and its reorganization energy is shared among two vibrations with slightly different frequencies. If the splitting is small compared to the resonance width, the vibrational-excitonic resonance "reassembles" the coupled mode from the split modes. This phenomenon is intimately related to the way in which vibrational-excitonic resonance assembles a delocalized and maximally coupled anti-correlated vibration from two localized but less strongly coupled pigment vibrations.

We also consider two Franck-Condon (FC) active vibrational modes on each pigment, with one vibrational frequency resonant and the other slightly off-resonant with the excitonic energy gap. In this case, both anti-correlated modes mix with the exciton. In the absence of line-broadening, the linear absorption spectrum around the excitonic line corresponding to the electronically excited donor pigment would split into n + 1 lines, where n is the number of nearresonant, Franck-Condon active vibrational levels. Such splittings of higher excitons are obscured by the overall line shape in absorption, do not appear in the relaxed emission spectrum from the lowest exciton, and change with the electronic energy gap between pigments. These observations have implications for the interpretation of low temperature absorption, emission, line-narrowing, and hole-burning spectroscopies.

II. THEORY

A. Hamiltonian

The dimer model used here has an electronic ground state (no pigments excited) and two singly excited states (one pigment excited). It also has one set of harmonic vibrations common to all three electronic states, which includes vibrations of both pigments plus vibrations of the surrounding protein. Taking the ground state geometry as a reference, these vibrations are linearly displaced upon electronic excitation. In a diabatic basis of localized pigment excitations, the dimer Hamiltonian for the ground and singly excited electronic states can be written in the form

$$\hat{H}_{dimer} = \sum_{i} \frac{1}{2} \omega_{i} (\hat{q}_{i}^{2} + \hat{p}_{i}^{2}) \hat{I}_{dimer}$$

$$+ \left(E^{A} + \frac{1}{2} (\mathbf{c}_{d} + \mathbf{g}_{d}^{A-B}) \cdot \hat{\mathbf{q}} \right) |A\rangle |G_{B}\rangle \langle G_{B}| \langle A|$$

$$+ \left(E^{B} + \frac{1}{2} (\mathbf{c}_{d} - \mathbf{g}_{d}^{A-B}) \cdot \hat{\mathbf{q}} \right) |G_{A}\rangle |B\rangle \langle B| \langle G_{A}|$$

$$+ J [|A\rangle |G_{B}\rangle \langle B| \langle G_{A}| + |G_{A}\rangle |B\rangle \langle G_{B}| \langle A|]. \quad (1)$$

In Eq. (1), \hat{I}_{dimer} is the identity operator for the dimer, which includes the ground state and the two excited states on the second and third lines. The coupling J between excited pigments appears on the last line. The ith harmonic oscillator has frequency ω_i and dimensionless coordinate operator \hat{q}_i with conjugate momentum \hat{p}_i . E^A and E^B are the excitation energies for the electronically excited states localized on pigments A and B, respectively, which may differ if the pigments are in non-equivalent sites in the protein. Right superscripts indicate belonging to an electronic state or states, while subscripts (except d for diabatic) indicate belonging to a pigment or vibrational mode. The pigment excitation energy gap (at $\mathbf{q} = 0$) is $\Delta = E^B - E^A$. The vector operator $\hat{\mathbf{q}} = \{\hat{q}_i\}$ is dotted into diabatic correlation $\mathbf{c}_d = \{-\omega_i(d_i^A + d_i^B)\}$ and tuning vectors $\mathbf{g}_d^{A-B} = \{-\omega_i(d_i^A - d_i^B)\}$ that quantify the equilibrium displacement for each vibrational mode upon electronic excitation of a pigment $(d_i^A \text{ or } d_i^B)$. Upon transformation [see Eq. (9) of Paper I¹¹] to the diabatic exciton basis $\{\alpha,\beta\}$ that diagonalizes the coupling at $\mathbf{q} = 0$, the excited state Hamiltonian

$$\hat{H}'_{dimer} = \sum_{i} \frac{1}{2} \omega_{i} (\hat{q}_{i}^{2} + \hat{p}_{i}^{2}) \hat{I}_{dimer}$$

$$+ \left(E^{\alpha} + \frac{1}{2} (\mathbf{c}_{d} + \mathbf{g}_{d}^{A-B} \cos(2\theta_{d})) \cdot \hat{\mathbf{q}} \right) |\alpha\rangle |G_{\beta}\rangle \langle G_{\beta}| \langle \alpha|$$

$$+ \left(E^{\beta} + \frac{1}{2} (\mathbf{c}_{d} - \mathbf{g}_{d}^{A-B} \cos(2\theta_{d})) \cdot \hat{\mathbf{q}} \right) |G_{\alpha}\rangle |\beta\rangle \langle \beta| \langle G_{\alpha}|$$

$$+ (\mathbf{g}_{d}^{A-B} \sin(2\theta_{d}) \cdot \hat{\mathbf{q}}) / 2 \left[|\alpha\rangle |G_{\beta}\rangle \langle \beta| \langle G_{\alpha}|$$

$$+ |G_{\alpha}\rangle |\beta\rangle \langle G_{\beta}| \langle \alpha| \right], \tag{2}$$

where the excitonic energies are

$$E^{\beta}_{\alpha} = [(E^B + E^A)/2] \pm \sqrt{(\Delta/2)^2 + J^2}$$

and $2\theta_d = \arctan[2J/\Delta]$

which gives the diabatic excitonic mixing angle θ_d . (Note that this is a different diabatic exciton basis from that described in Ref. 12.) The excitonic energy gap (at $\mathbf{q} = 0$) is $\Delta^{EX} = E^{\beta} - E^{\alpha}$. In terms of the uncoupled monomer electronic transition dipole vectors $\boldsymbol{\mu}_{GA}$ and $\boldsymbol{\mu}_{GB}$, the diabatic exciton transition dipole vectors are

$$\mathbf{\mu}_{G\alpha} = \cos(\theta_d)\mathbf{\mu}_{GA} - \sin(\theta_d)\mathbf{\mu}_{GB}$$

and

If the monomer transition dipoles have a parallel component, interference will alter the excitonic transition strengths (for example, H vs. J aggregates in which the upper vs. lower exciton takes all the absorption strength¹³). If the monomer transition dipoles have perpendicular components, interference will rotate the excitonic transition dipoles in the molecular frame. In some aggregates, monomer transition dipoles have parallel and perpendicular components, and both excitons have absorption strength (these are sometimes called HJ aggregates ¹⁴). For equal magnitude perpendicular monomer transition dipoles, excitonic coupling generates a pure rotation of the transition dipoles (by up to 45°) in the molecular frame; both excitonic transitions have the same total dipole strength as a monomer, independent of the coupling. The electronically off-diagonal coupling on the last line of Eq. (2) mixes vibrational levels across the two excitons so that vibronic transitions in the stick spectrum have transition dipole moments with various magnitudes and rotation angles.

The correlation vector tunes both excitonic energies relative to the ground state in exactly the same way that it tuned both pigment excitation energies. Only the tuning vector is affected by the transformation, with an attenuated role in tuning the excitonic energy gap and a new role in excitonically off-diagonal vibronic coupling. The term on the last line of the Hamiltonian in the diabatic excitonic basis shows that vibrational-excitonic mixing can only happen through the anticorrelated nuclear motions which tune the energy gap between the singly excited states of the two pigments.

In general, the correlation and tuning vectors are not orthogonal. For example, an environmental mode k that is displaced by d_k only upon excitation of pigment A makes an equal contribution of $-\omega_k d_k$ to both vectors (adding to $-2\omega_k d_k$ for A and subtracting to 0 for B). For intramolecular modes, it is useful to transform the normal modes localized on the pigments into delocalized normal modes. For equal localized mode frequencies ω_i and equal positive displacements d_i , correlated vibrations $\hat{q}_{j+} = (\hat{q}_{jA} + \hat{q}_{jB})/2^{1/2}$ contribute only to \mathbf{c}_d while delocalized anti-correlated vibrations $\hat{q}_{j-} = (\hat{q}_{jA} - \hat{q}_{jB})/2^{1/2}$ contribute only to \mathbf{g}_d^{A-B} (both contributions are equal in magnitude to $\omega_i \sqrt{2}d_i$). This transformation is advantageous because only the anti-correlated vibrations are directly coupled to the nonadiabatic energy transfer dynamics, though asymmetric environmental modes must also be included in the nonadiabatic Hamiltonian.

B. Quantum vibrational states for delocalized vibrations

The quantum nature of the delocalized vibrations is important for the energy transfer process. Here, we illustrate the nature of the delocalized vibrational quantum states using a common, localized vibrational basis on all electronic states. The diabatic excitonic basis is used for the electronic states. In this subsection, for simplicity, the equilibrium harmonic oscillator vibrational basis of the ground electronic state is used for both excitonic states (so vibrational states do not have an electronic superscript here). This simplification is fairly accurate because the equilibrium displacements are small compared to zero point vibrational amplitude in chlorophylls so that the resonant couplings between vibrational levels on different electronic states cause the most significant changes in the quantum states.

For illustration, we consider a single vibrational mode on both pigments with identical displacements d. The lowest vibrational state of the singly excited dimer is the isolated vibrational zero point level of the excitonic acceptor state, $|\alpha\rangle | v_A = 0 \rangle | v_B = 0 \rangle$, which has diagonal energy $E_0^\alpha = E^\alpha + \omega$ (zero point energy from two vibrations). Near vibrational-excitonic resonance, $\omega \approx \Delta^{EX}$, and the next three basis states have approximately isoenergetic diagonal energies: the two vibrational basis states $|\alpha\rangle | v_A = 1 \rangle | v_B = 0 \rangle$ and $|\alpha\rangle | v_A = 0 \rangle | v_B = 1 \rangle$ on the lower energy exciton both have diagonal energy $E_0^\alpha + \omega$; the zero point vibrational level of the excitonic donor state, $|\beta\rangle | v_A = 0 \rangle | v_B = 0 \rangle$, has diagonal energy $E_0^\beta = E_0^\alpha + \Delta^{EX} \approx E_0^\alpha + \omega$. We now consider only the part of the Hamiltonian matrix

We now consider only the part of the Hamiltonian matrix in Eq. (2) that directly couples these three isoenergetic basis states and neglect their coupling to other basis states as a perturbation. For the single vibrational mode, the tuning vector operator simplifies to $\mathbf{g}_d^{A-B} \cdot \hat{\mathbf{q}} = -\omega d(\hat{q}_A - \hat{q}_B)$. The nonzero matrix elements of the vibrational coordinate operators are $\langle v_X | \hat{q}_X | v_X + 1 \rangle = \sqrt{(v_X + 1)/2}$ and its Hermitian conjugate. The vibrationally diagonal matrix elements of $\mathbf{g}_d^{A-B} \cdot \hat{\mathbf{q}} \cos(2\theta_d)/2$ are zero and the first basis two states on the acceptor are not directly coupled to each other by $\mathbf{g}_d^{A-B} \cdot \hat{\mathbf{q}} \cos(2\theta_d)/2$ because there is a simultaneous change in both vibrational quantum numbers between them. However, both are directly coupled to the zero point basis state on the donor by the electronically and vibrationally off-diagonal operator $+\mathbf{g}_d^{A-B} \cdot \hat{\mathbf{q}} \sin(2\theta_d)/2$, which has vibrational matrix elements

$$\langle v_B = 0 | \langle v_A = 0 | + \mathbf{g}_d^{A-B} \cdot \hat{\mathbf{q}} \sin(2\theta_d) / 2 | v_A = 1 \rangle | v_B = 0 \rangle$$
$$= -\omega d \sin(2\theta_d) / 2\sqrt{2}$$

and

$$\langle v_B = 0 | \langle v_A = 0 | + \mathbf{g}_d^{A-B} \cdot \hat{\mathbf{q}} \sin(2\theta_d)/2 | v_A = 0 \rangle | v_B = 1 \rangle$$

= $+\omega d \sin(2\theta_d)/2\sqrt{2}$.

Thus, the part of the Hamiltonian matrix \hat{H} coupling the three isoenergetic states in the vibrationally localized vibrational-exciton basis becomes, in the (shorthand $\mu v_A v_B$) basis $\{\alpha 0_A 1_B, \alpha 1_A 0_B, \beta 0_A 0_B\}$,

$$\hat{H} = \begin{bmatrix} E_0^{\alpha} + \omega & 0 & +\omega d \sin(2\theta_d)/2\sqrt{2} \\ 0 & E_0^{\alpha} + \omega & -\omega d \sin(2\theta_d)/2\sqrt{2} \\ +\omega d \sin(2\theta_d)/2\sqrt{2} & -\omega d \sin(2\theta_d)/2\sqrt{2} & E_0^{\beta} \end{bmatrix}.$$
 (3)

Under the transformation U,

$$U = \begin{bmatrix} 1/\sqrt{2} & -1/\sqrt{2} & 0\\ 1/\sqrt{2} & 1/\sqrt{2} & 0\\ 0 & 0 & 1 \end{bmatrix}, \tag{4}$$

the matrix in Eq. (3) transforms to

$$U^{\dagger} \hat{H} U = \begin{bmatrix} E_0^{\alpha} + \omega & 0 & 0 \\ 0 & E_0^{\alpha} + \omega & -\omega d \sin(2\theta_d)/2 \\ 0 & -\omega d \sin(2\theta_d)/2 & E_0^{\beta} \end{bmatrix}.$$
(5)

The zero-point excitonic donor basis state $|\beta\rangle |v_A=0\rangle |v_B=0\rangle$ is coupled only to the antisymmetric superposition of the two vibrationally excited excitonic acceptor basis states $|\alpha\rangle (|v_A=1\rangle |v_B=0\rangle - |v_A=0\rangle |v_B=1\rangle)/\sqrt{2}$. Further, the donor coupling to the one antisymmetric vibrational superposition is increased by a factor of $\sqrt{2}$ compared to the donor coupling to either of the two localized vibrational states.

The vibrational part of these vibrational-electronic states can be understood from the viewpoint of delocalized vibrational modes. Using the vibrational wavefunctions $\langle q_X | \nu_X \rangle$ where $|q_X\rangle$ is the position ket corresponding to a vibration of pigment X, and the correlated $\hat{q}_+ = (\hat{q}_A + \hat{q}_B)/2^{1/2}$ and anticorrelated $\hat{q}_- = (\hat{q}_A - \hat{q}_B)/2^{1/2}$ delocalized coordinates, one can show that

$$|\alpha\rangle |\nu_{+} = 1\rangle |\nu_{-} = 0\rangle = |\alpha\rangle [|\nu_{A} = 0\rangle |\nu_{B} = 1\rangle + |\nu_{A} = 1\rangle |\nu_{B} = 0\rangle]/\sqrt{2},$$

$$|\alpha\rangle |\nu_{+} = 0\rangle |\nu_{-} = 1\rangle = |\alpha\rangle [|\nu_{A} = 1\rangle |\nu_{B} = 0\rangle - |\nu_{A} = 0\rangle |\nu_{B} = 1\rangle]/\sqrt{2},$$

$$|\beta\rangle |\nu_{+} = 0\rangle |\nu_{-} = 0\rangle = |\beta\rangle |\nu_{A} = 0\rangle |\nu_{B} = 0\rangle.$$
(6)

The transformed matrix in Eq. (5) shows how the first state in Eq. (6), with a quantum of excitation along the correlated vibrational coordinate \hat{q}_+ , is decoupled from the other two isoenergetic states. Only a quantum of excitation along the anti-correlated vibrational coordinate \hat{q}_- on exciton $|\alpha\rangle$ is coupled to the higher energy exciton $|\beta\rangle$. At vibrational-excitonic resonance, the eigenstates around one vibrational quantum of excess energy are approximately

$$\begin{aligned} |\alpha\rangle |\nu_{+} &= 1\rangle |\nu_{-} &= 0\rangle, \\ |(1+0)\rangle &= \left[|\alpha\rangle |\nu_{+} &= 0\rangle |\nu_{-} &= 1\rangle + |\beta\rangle |\nu_{+} &= 0\rangle |\nu_{-} &= 0\rangle \right] / \sqrt{2}, \\ |(1-0)\rangle &= \left[|\alpha\rangle |\nu_{+} &= 0\rangle |\nu_{-} &= 1\rangle - |\beta\rangle |\nu_{+} &= 0\rangle |\nu_{-} &= 0\rangle \right] / \sqrt{2}. \end{aligned} \tag{7}$$

The first state is partially electronically delocalized by the non-resonant excitonic coupling and fully vibrationally delocalized but vibronically decoupled. The last two states are fully electronically and vibrationally delocalized 50:50 mixtures of vibronically coupled basis states. In the shorthand notation on the left, the 1 and 0 represent the anti-correlated quantum numbers on α and β , respectively. The physical picture is that coupling to localized vibrations on both donor and acceptor pigments decouples a delocalized correlated vibration and assembles a delocalized anti-correlated vibration with all of the coupling. This delocalized anti-correlated vibration drives energy transfer and is driven by energy transfer but need not survive after energy transfer.

Figure 1 shows a vibronic energy level mixing diagram for an excitonically coupled non-degenerate $(E^A \neq E^B)$ homodimer with one vibrational mode per pigment. The nested potential surfaces for this model can be seen in Fig. 1 of Ref. 15. The model parameters are taken from Ref. 2 and roughly mimic one of the interpigment interactions in the Fenna-Matthews-Olson (FMO) antenna complex from green sulfur bacteria. ¹⁶ Figure 1 shows all vibronic levels with up to one vibrational quantum

on the dimer with an electronically excited donor and up to two vibrational quanta on the dimer with an electronically excited acceptor. The energies of the localized vibrations of the uncoupled dimer [ignoring the electronically off-diagonal terms in Eq. (1)] are given at the far left and far right. Excitonic coupling gives rise to diabatic exciton states [obtained by ignoring the electronically (and vibrationally) off-diagonal terms in Eq. (2)] that have a systematic pattern of vibronic level degeneracies (vibrational excitonic resonances). The energies of the exact nonadiabatic eigenstates are given in the middle along with their approximate vibrational-excitonic character as determined by diagonalizing a Hamiltonian sub-matrix of degenerate states. The approximate state labels include direct couplings through the electronically and vibrationally offdiagonal coupling on the last line of Eq. (2) but neglect indirect couplings from the electronically diagonal but vibrationally off-diagonal terms that cause the reorganization energy [on the second and third lines of Eq. (2)]. For the zero point donor, the degenerate Hamiltonian sub-matrix has 3 states [as in Eqs. (3)–(7)]. For a dimer with one vibrational quantum and electronic excitation on the donor, the degenerate sub-matrix has 5 states. Excitation of the anti-correlated vibration on the donor makes the vibrational excitonic resonance a factor of $\sqrt{2}$ stronger (this larger splitting can also be seen in Fig. 1 of Ref. 2 and all 5 eigenstates can be seen in Fig. 2 of Ref. 17 for different parameters). This increase follows from the $\sqrt{v+1}$ scaling of the matrix elements of the vibrational coordinate operators. More generally, excitation of the anti-correlated vibration promotes nonadiabatic coupling, while excitation of the correlated vibration has no effect.

The above treatment should be contrasted with the coherent exciton scattering (CES) approximation used for polymers¹⁸ and the "one-particle" vibronic-exciton model used for molecular crystals;^{9,19} both assume that vibrational excitation follows electronic excitation and omit the state

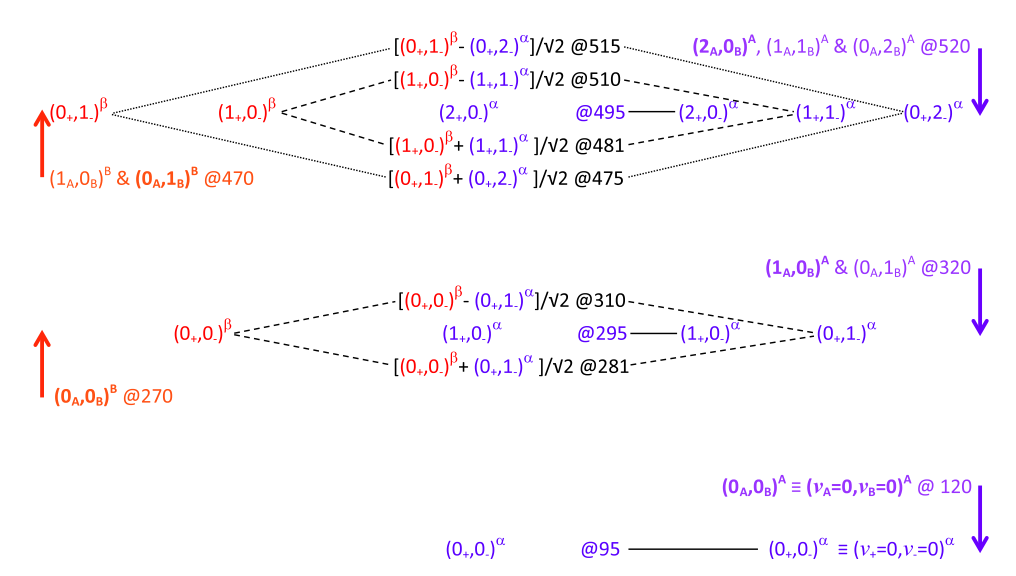


FIG. 1. Vibronic energy level diagram for the one-exciton states of a non-degenerate homodimer with vibrational-excitonic resonance. The uncoupled pigment site energies are $E^A = -75 \text{ cm}^{-1}$ and $E^B = +75 \text{ cm}^{-1}$ with coupling $J \approx 66.14 \text{ cm}^{-1}$ such that the excitonic energy gap $\Delta^{EX} = 200 \text{ cm}^{-1}$ is resonant with one intramolecular vibration at $\omega = 200 \text{ cm}^{-1}$. The vibrational displacements are $d^A = d^B \approx 0.224$, which lowers all energy levels by the reorganization energy $\lambda = (1/2)\omega d^2 = 5 \text{ cm}^{-1}$ for electronic excitation of a pigment. The abbreviated quantum state labels are defined at lower right and enclose the set of vibrational quantum numbers with subscripts that indicate the mode inside parentheses, with a right superscript for the electronic state. Localized pigment states and energies (in the absence of the coupling J) are given at the far left for the donor B (orange-red) and the far right for the acceptor A (violet). Among these states, the states that appear in the coherent exciton scattering approximation or one-particle approximation of the vibronic exciton model are set in boldface type. In the diabatic exciton approximation, all states with an electronically excited donor β (red) are shifted up 25 cm⁻¹ by excitonic coupling (red arrow), while all states with an electronically excited acceptor α (blue) are shifted down 25 cm⁻¹ (blue arrow). The energy levels in the middle were obtained by diagonalization of the Hamiltonian in Eq. (1) using a basis set that included all states with $v_A \le 9$ and $v_B \le 9$. The approximate state labels in the middle reflect only resonant vibrational-excitonic mixing from the direct electronically and vibrationally off-diagonal coupling in Eq. (2). For each state, the energy in cm⁻¹ is rounded off to the nearest integer and indicated after the @. Relative to the diabatic exciton basis states, the electronically off-diagonal coupling in Eq. (2) does not affect acceptor exciton states in which only the correlated vibration is excited. For these states, the exact nonadiabatic energy given in the middle also specifies the energy of all diabatic exciton basis states shown on the same level. For each state in the middle panel, the contributing diabatic exciton states (red and blue) are indicated by solid lines (when the highest anti-correlated vibrational quantum number contributing to the eigenvector is 0), dashed lines (when the highest anti-correlated vibrational quantum number contributing to the eigenvector is 1), or dotted lines (when the highest anti-correlated quantum number contributing to the eigenvector is 2).

 $|\alpha\rangle |v_A=0\rangle |v_B=1\rangle$ in which the acceptor is electronically excited but vibrational excitation remains behind on the donor. As discussed in Paper I,¹¹ these approximations reduce the energy transfer rate by a factor of 2. This factor of 2 error can be understood in two ways: from the perspective of delocalized vibrations, only the anti-correlated vibrational coordinate is coupled to electronic energy transfer, but with a factor of $\sqrt{2}$ greater coupling [Eq. (5)]; from the perspective of localized vibrations, the coupling is independent of whether the vibrational excitation follows the electronic excitation or is left behind [equal magnitude matrix elements in Eq. (3)], so there are two equally probable energy transfer products. The channel with vibration on the donor and electronic excitation on the acceptor represents dissociation of a "vibronic exciton." ^{19,20} Since the concept of a "vibronic exciton" was developed as the excitonic analog of a polaron ("excitaron," 20 "excitonic polaron,"21 and "Frenkel polaron"8), in which a lattice distortion adiabatically follows a charge, the name is not accurate when dissociation is so probable.

Figure 1 also shows that the "one-particle" approximation of the vibronic exciton model fails in another way to capture the role of vibration in promoting energy transfer. Although there are 5 states with energy approximating that for an electronically excited donor with one vibrational quantum, there are only two "one particle" states around this energy $|B\rangle |v_A = 0\rangle |v_B = 1\rangle$ and $|A\rangle |v_A = 2\rangle |v_B = 0\rangle$]. Because their

corresponding vibrational quantum numbers differ by more than one, these two states are not *directly* coupled to each other through the electronically off-diagonal coupling in Eq. (2). As a result, the "one-particle" approximation of the vibronic exciton model incorrectly yields smaller splittings (from *indirect* couplings—see the supplementary material) as vibrational excitation increases. This failure of the "one-particle" approximation for electronic absorption spectra has been previously discussed by Spano²² and impacts the vibrational progressions in Ref. 14. For energy transfer, the "one-particle" approximation leads to the qualitatively incorrect conclusion that vibrational excitation would slow nonadiabatic energy transfer.

In spectroscopy, if perturbation theory is applicable to the energy transfer coupling, the CES approximation and "one-particle" vibronic exciton model incorrectly reduce the absorption intensity borrowed through the energy transfer coupling by a factor of 2. This factor also extends the width of the vibrational excitonic resonance, which impacts both the spectroscopy and energy transfer dynamics of the dimer. In a full non-adiabatic treatment, such vibrational-excitonic resonance generates eigenstates that are both electronically and vibrationally delocalized, with rapid changes in electronic character as a function of the anti-correlated vibrational coordinate. The mixed states that result from diagonalizing the interacting 2×2 sub-matrix in Eq. (5) provide a low order description of these states and the vibrational-excitonic resonance

criterion that is much simpler but slightly less accurate than the non-adiabatic treatment of Ref. 2. This sub-section has simply and approximately illustrated a rigorous, symmetry dictated decoupling of the correlated coordinate and enhanced coupling to the anti-correlated coordinate that occur in any correct treatment of the problem. As will be seen below, the resolved 1D spectra directly reflect both decoupling of the correlated vibration and enhanced energy transfer coupling through the anti-correlated vibration.

C. Huang-Rhys factors for delocalized vibrations

The evaluation of Franck-Condon factors makes a displaced vibrational basis set on each electronic state more natural than the common vibrational basis set of the ground electronic state used above. In this paper, intramolecular vibrational displacements upon electronic excitation are identical for the uncoupled pigments so that the correlated and anticorrelated vibrations become symmetric and anti-symmetric under pigment exchange. As in Paper I,¹¹ a right superscript $(0, \alpha, \text{ or } \beta)$ will be used to denote the electronic state for displaced vibrational basis states. All vibrations on the ground electronic state 0 have their equilibrium at zero displacement. $\left|v_{j+}^{\alpha}=0\right\rangle$ and $\left|v_{j+}^{\beta}=0\right\rangle$ are the kets for the correlated vibrational basis states with $v_{j+}=0$ on the diabatic potentials for excitons α and β , respectively; both have their equilibrium at $d_{i+} = d_i/\sqrt{2}$, where d_i is the positive equilibrium displacement for mode j upon electronic excitation for either isolated pigment. $|v_{j-}^{\alpha}=1\rangle$ and $|v_{j-}^{\beta}=1\rangle$ are the kets for the anti-correlated vibrational basis states with $v_{j-}=1$ on the diabatic potentials for excitons α and β , respectively; these have equal and opposite equilibrium displacements of $d_{i-}^{\alpha} = d_j \cos(2\theta_d)/\sqrt{2}$ and $d_{i-}^{\beta} = -d_{i}\cos(2\theta_{d})/\sqrt{2}$. The anti-correlated displacements are reduced to their localized electronic state probability weighted average by excitonic mixing. These displaced basis states are eigenstates of the Hamiltonian in Eq. (2) when the electronically off-diagonal coupling $(\mathbf{g}_d^{A-B}\sin(2\theta_d)\cdot\hat{\mathbf{q}})/2$ between excitons is neglected.

Symmetric correlated vibrations have the same pattern of displacements as a totally symmetric vibration in a Jahn-Teller system, and Franck-Condon vibrational overlap integrals can be evaluated using Eqs. (8)–(15) of Ref. 23. Anti-symmetric anti-correlated vibrations have the same pattern of displacements as Jahn-Teller active vibrations so that Franck-Condon overlap integrals can be evaluated using Eqs. (16)–(27) of Ref. 23. In linear spectra, the adiabatic intensities depend on the ratio of Franck-Condon factors

$$S_{jm}^{\mu-G} = \left| \left\langle v_{jm}^G = 0 \middle| v_{jm}^{\mu} = 1 \right\rangle \right|^2 / \left| \left\langle v_{jm}^G = 0 \middle| v_{jm}^{\mu} = 0 \right\rangle \right|^2 = (d_{jm}^{\mu})^2 / 2, \tag{8}$$

where j indicates the intramolecular mode number, $m = \{+,-\}$ indicates the correlated or anti-correlated delocalized vibration, and $\mu = \{\alpha,\beta\}$ indicates the diabatic exciton. For equal frequency harmonic vibrations on both electronic states, the ratio $S_{jm}^{\mu-G}$ is known as the Huang-Rhys factor and has the value given by the last equality.²⁴ The Huang-Rhys factors give exact intensity ratios for adiabatically separable harmonic vibrations even when the Franck-Condon principle fails for the overall vibrational-electronic state. A correlated vibration's

Huang-Rhys factor is exactly half of that for the isolated pigment vibration

$$S_{j+}^{\alpha-G} = S_{j+}^{\beta-G} = (d_{j+})^2/2 = (d_j/\sqrt{2})^2/2$$
$$= S_j^{A-G}/2 = S_j^{B-G}/2.$$
(9a)

The anti-correlated vibrations' Huang-Rhys factors are each less than that of the corresponding correlated vibration by a factor of $\cos^2(2\theta_d)$,

$$S_{j-}^{\alpha-G} = S_{j-}^{\beta-G} = (d_{j-})^2/2 = (d_j \cos(2\theta_d)/\sqrt{2})^2/2$$
$$= S_i^{A-G} \cos^2(2\theta_d)/2 = S_i^{B-G} \cos^2(2\theta_d)/2.$$
(9b)

In the diabatic exciton approximation, Eq. (9) shows that the sum of the Huang-Rhys factors for the correlated and anti-correlated delocalized vibrations lies in the range

$$S_i^{A-G}/2 \le S_{i+}^{\alpha-G} + S_{i-}^{\alpha-G} \le S_i^{A-G}.$$
 (10)

This sum is greater than or equal to half of the Huang-Rhys factor for the localized vibration on an isolated pigment, becoming equal for complete excitonic delocalization (as occurs in degenerate homodimers³). This sum is also less than or equal to the isolated pigment vibration's Huang-Rhys factor, becoming equal in the absence of excitonic mixing. Such reductions in Huang-Rhys factors 12,25 from excitonic delocalization are well known,³ but the explanation in terms of reduced displacements for correlated and anti-correlated vibrations is new and has consequences for resonances. Such reduced displacements are related to the $1/N_{coh}$ reduction in strength for vibronic bands in aggregate photoluminescence³ treated by Spano and Yamagata.²⁶ The totally symmetric phonon in the aggregate there corresponds to the correlated vibration here so that 1/Nfor the degenerate aggregate generalizes 1/2 for the correlated vibration of the dimer. The vibrational-excitonic resonance in a non-degenerate homodimer treated here was explicitly excluded in the treatment of disorder by Ref. 26. It provides a different perspective on disorder in an aggregate: here the 0-0 linestrength is *almost unaffected* by excitonic delocalization because the monomer transition dipoles are perpendicular (so that the total excitonic strengths are unaffected by delocalization) while the Huang-Rhys factor (hence 0-1 emission linestrength) for the anti-correlated vibration is reduced by exciton delocalization, but not zeroed; in Ref. 26, for parallel transition dipoles the 0-0 linestrength growth slows from N to N_{coh} through disorder-induced localization while the 0-1 emission linestrength is unaffected. Schulze et al. have noted similar monomer dipole arrangement effects.²⁵ Womick and Moran have presented an inverse participation ratio (or participation number) that generalizes the coherence length for vibrational-excitonic mixing.²⁷

The displaced basis states for the correlated vibration are eigenstates of the adiabatic excitons and of the full non-adiabatic Hamiltonian—their Franck-Condon factors show up directly in the 1D spectra. By contrast, the eigenstates of the anti-correlated vibration become anharmonic in the adiabatic approximation (requiring use of the more general Franck-Condon factors) and can become vibronically entangled with the excitons [see Eq. (7)] so that the Franck-Condon principle fails. All these effects are treated exactly in the numerical calculations below.

III. MODELS AND RESULTS

Vibrational-excitonic resonance can alter the intensities of vibrational-electronic transitions so that they do not reflect the Franck-Condon vibrational overlap factors given by the displacement of vibrational equilibrium between electronic states. Consideration of the vibrational-excitonic resonance hypothesis requires an analysis of how it affects the interpretation of all spectroscopic experiments. For this reason, we prefer to start calculations with the displacements determined from Franck-Condon analysis of the intensities in the isolated pigment, where vibrational-excitonic resonance is absent.

The approach adopted here is based on a second hypothesis that large changes in vibrational-electronic intensities between isolated pigment and antenna are primarily caused by excitonic delocalization and vibrational-excitonic resonance rather than by perturbations of single pigment properties in specific protein sites, which also undoubtedly occur. If this hypothesis is correct, displacements determined from antenna vibronic intensities without taking the vibrational-excitonic resonance into account may be seriously in error. In FMO, Freiberg and co-workers have ascribed changes in effective Huang-Rhys factors across exciton bands to energy transfer, ^{28,29} and Schulze *et al.* have discussed excitonic effects. ²⁵ Ultimately, excitonic delocalization, vibrational-excitonic resonance, and site-specific protein effects on vibrational frequencies^{30,31} and on vibrational displacement upon electronic excitation^{31,32} must all be considered in order to synthesize models that consistently treat both isolated pigments and each specific antenna protein. This second hypothesis adopted here is not meant to be exact and must be judged on its fruits as a starting point in individual cases.

Based on the small displacements in vibrational equilibrium upon electronic excitation in the isolated $BChl\ a$ pigment $(d^2\ll 1)$, the absence of vibrational progressions in the Q_y -band electronic spectra of $BChl\ a$ suggests that distinct and similarly intense peaks in the vibrationally unresolved Q_y -band electronic absorption spectra of FMO should roughly reflect excitonic basis state energies. It will be shown below that this assumption, used in prior modeling of the FMO linear and circular dichroism spectra with excitonic Hamiltonians, 16 remains valid for FMO on the hypothesis of vibrational-excitonic resonance. Thus, linear absorption spectra provide a starting point for determining excitonic energy gaps here.

For FMO, the low temperature absorption spectrum 16,33,34 clearly shows that there is an exciton ~ 165 cm⁻¹ above the transition to the lowest observed exciton. Resonance Raman, 35 fluorescence line-narrowing, 28,36 and hole-burning 37 experiments have shown a FC active vibration of the *BChl a* pigment with $\omega/2\pi c \sim 165$ cm⁻¹. As a result, the v=1 level of this vibration on the lowest observed exciton is resonant with the v=0 level of the higher exciton. Here, resonance is modeled for a ~ 200 cm⁻¹ vibrational frequency and excitonic splitting; 4 excitonic models that predate 2D spectroscopy on FMO give excitonic splittings (between the 2nd and 5th excitons—see models B, C, D, and E in Table 7 of Ref. 16) of 190-210 cm⁻¹, while resonance Raman, 35 fluorescence line

narrowing, ^{28,36} and hole burning ³⁷ experiments all find a ~195 cm⁻¹ FC active vibration of the *BChl a* pigment. Neither the pigment site energies nor the Coulombic couplings are directly known from experiment, only the excitonic energy gap. Electronic coupling between different pigment sites in the FMO antenna protein can range from ~30 to 110 cm⁻¹. ^{16,38–40} The average site energy gap $\langle \Delta \rangle = 150 \, \text{cm}^{-1}$ and Coulombic coupling $J = 66.14 \, \text{cm}^{-1}$ are chosen to reproduce the average energy gap between the excitons, $\langle \Delta^{EX} \rangle = \langle 2[(\Delta/2)^2 + J^2]^{1/2} \rangle = 200 \, \text{cm}^{-1}$.

 $\langle \Delta^{EX} \rangle = \langle 2[(\Delta/2)^2 + J^2]^{1/2} \rangle = 200 \text{ cm}^{-1}$. A second key model parameter is the anti-correlated inhomogeneity in site energies, which is quantified by $\sigma_{\Delta} = \langle (\Delta - \Delta_0)^2 \rangle^{1/2}$, where $\Delta = (E^B - E^A)$ is the excitation energy gap between pigments in one protein, $\Delta_0 = \langle \Delta \rangle$ is the ensemble average excitation energy gap, and the brackets indicate averaging over the ensemble of proteins. The femtosecond pump-probe polarization anisotropy decay of FMO measured by Savikhin, Buck, and Struve determined this for one pair of excitons at 19 K. They reported strong quantum beats with ~220 fs period decaying on a ~140-180 fs time scale in the anisotropy, attributed the beats to coherence between excitons, and attributed the decay to the distribution of excitonic energy gaps, finding $\sigma_{\Delta EX} = 34 \text{ cm}^{-1}$. As explained in Ref. 2, this distribution is narrower than the underlying distribution of site energies, giving $\sigma_{\Delta} = 45 \text{ cm}^{-1}$ for the average site energy gap and coupling used here.

A. Dimer with one intramolecular vibrational mode per pigment

The special case of one FC-active vibrational mode on each pigment, with identical frequencies ω and positive FC displacements d, has been treated in Ref. 2. The total single exciton Hamiltonian \hat{H}_1 is a sum of the correlated Hamiltonian \hat{H}_+ in Eq. (32) of Paper I ($\hat{H}_+ = \hat{H}_{corr}$ of Ref. 2) and the interaction Hamiltonian \hat{H}_- in Eq. (34) of Paper I ($\hat{H}_- = \hat{H}_{int}$ of Ref. 2). The generalized tuning vector gives $\mathbf{g}_d^{A-B} \cdot \hat{\mathbf{q}} = -\sqrt{2}\omega d\hat{q}_-$. Tiwari $et\ al.^2$ have shown that a single FC-active vibrational mode resonant with the excitonic energy gap of the dimer system can lead to strongly coupled nuclear and electronic states on the excited state of the dimer.

Model parameters are roughly based on one pair of excitons in the Fenna-Matthews-Olson (FMO) complex from green sulfur bacteria ¹⁶ and are identical to those used in Ref. 2. In the dimer model, the transition dipoles of the two pigments are perpendicular and are assumed to be of equal strength. The FC active vibrational frequency of $\omega/2\pi c = 200$ cm⁻¹ and dimensionless displacement of d = 0.22 are based on the \sim 3-5 cm⁻¹ reorganization energy [$\lambda_{vib} = (1/2)\omega d^2 \approx 5$ cm⁻¹] reported in various fluorescence line-narrowing studies on *BChl* $a.^{28,34,36}$

Broadening due to the low-frequency phonon sideband of FMO protein and other low frequency vibrations of BChl a is incorporated using a Brownian oscillator that introduces an effective damping of the coherence between the ground and singly excited state and therefore broadens the absorption line shapes. A critically damped Brownian oscillator with a frequency of 70 cm $^{-1}$ and an effective reorganization energy

of $\lambda_{eff} = 30 \text{ cm}^{-1}$ is used. When a pigment vibration with $\lambda_{vib} = 5 \text{ cm}^{-1}$ is incorporated, this reproduces the total reorganization energy of $\lambda_{tot} = 35 \text{ cm}^{-1} \text{ used in some models}^{38}$ for 2D spectra of FMO. The low temperature Stokes' shift of 22 cm⁻¹ between absorption and emission maxima for the lowest exciton in stable FMO proteins⁴² is attributed mainly to environmental protein phonons^{28,43} ($\lambda_{env} \approx 11 \text{ cm}^{-1}$). A sum of reorganization energies for low frequency BChl a vibrations ($\nu \le 500 \text{ cm}^{-1}$) from Ref. 36 accounts for the rest. This Brownian oscillator broadening is just an effective line shape that roughly accounts for a great many phonons and vibrations because it has a similar spectral density even if the dynamics are oversimplified.⁴⁴ For 1D spectra, the quantum Brownian oscillator line shape 45,46 can be incorporated by convolution with the stick spectrum calculated using Boltzmann eigenstate populations, the numerical eigenvalues, and transition dipoles calculated from numerical eigenvectors of the Hamiltonian^{2,47} in Eq. (1)—complete equations are given in the supplementary material.

The upper panel of Fig. 2 shows the absorption spectrum of the dimer model described above, but modified to set the Franck-Condon vibrational displacement to d=0. This modification eliminates the vibrational-electronic coupling to generate a purely electronically coupled dimer. The stick spectrum shows transition dipole strengths $|\mu_{if}|^2$ calculated from the dimer Hamiltonian and does not include line-broadening. The stick spectrum reveals two purely excitonic transitions with equal intensity.

The absorption cross section at a temperature of 80 K includes both line broadening from the Brownian oscillator model and the proportionality to frequency from the radiative excitation rate. Line broadening from the Brownian oscillator is strongly asymmetrical because it arises from vibrational-electronic transitions: thermal excitation of the Brownian oscillator mode is required for transitions with frequency below the line in the stick spectrum (hot bands), but not for transitions above the line. This blue-shifts both peaks in the absorption cross section. The proportionality to frequency and a slight asymmetry in the overlapping line shapes around their centers make the peak cross section around the transition to the higher energy exciton slightly greater than the peak cross section around the transition to the lower energy exciton.

The middle panel of Fig. 2 shows how the purely excitonic spectrum in the upper panel is modified by vibrational-excitonic resonance when the Franck-Condon vibrational displacement of the pigment vibration is $d \approx 0.22 \ [\lambda_{vib} = (1/2)\omega d^2 = 5 \ \text{cm}^{-1}]$. The underlying stick spectrum reveals that the upper excitonic transition has split into two strong lines of nearly equal dipole strength. Closer inspection of the stick spectrum shows that the transition to the lower exciton has been red-shifted by the 5 cm⁻¹ reorganization energy, λ_{vib} , of the pigment vibrational mode in the dimer Hamiltonian. The stick spectrum also shows a number of weaker lines (see below).

When a Brownian oscillator line shape is used to model line broadening due to the correlated part of the low-frequency phonon sideband in FMO, the absorption cross section (shown in gray) completely obscures the splitting seen in the stick

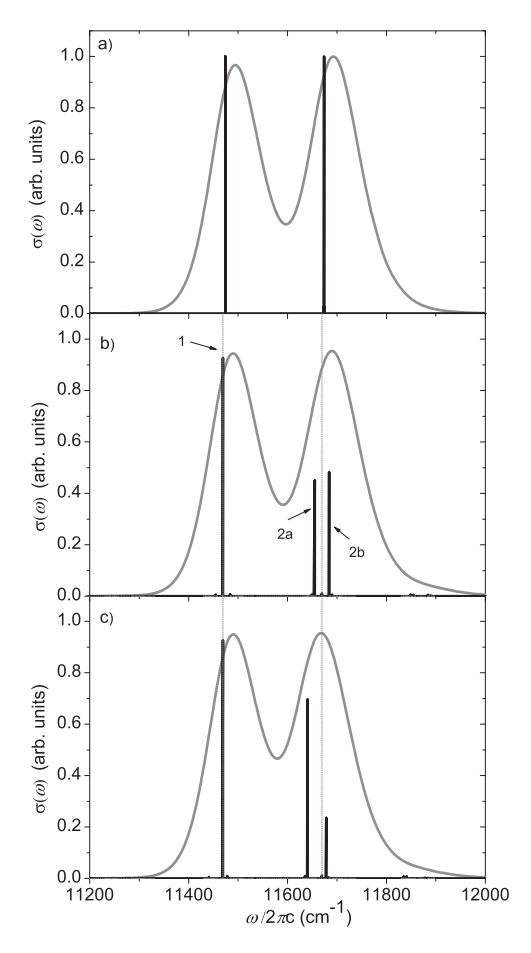


FIG. 2. Absorption cross section for a non-degenerate homodimer with a 90° angle between pigment transition dipoles and one FC active vibrational mode per pigment. Maximum peak intensity in the upper panel has been normalized to one and the peak intensities in the middle and lower panels are shown relative to the upper panel. In all panels, the average site excitation energy is $(E^A + E^B)/2 = 11\,574\,\mathrm{cm}^{-1}$ and the site energy gap between pigments is $\Delta = 150 \text{ cm}^{-1}$ with coupling $J = 66.14 \text{ cm}^{-1}$ such that the excitonic energy gap is $\Delta^{EX} = 200 \text{ cm}^{-1}$. The line shapes are calculated at a temperature T = 80 K using convolution with the line shape for a critically damped Brownian oscillator with a frequency of 70 cm⁻¹ and a reorganization energy of $\lambda_{eff} = 35 \text{ cm}^{-1} - \lambda_{vib}$. The line shape is then multiplied by frequency to generate the absorption cross-section. All cross sections are relative to peak 2, which is normalized to one at the maximum in panel (a). (a) Purely electronic coupling with $\lambda_{vib} = 0$. The lower and upper exciton peaks are at 11 474 cm⁻¹ and 11 674 cm⁻¹ in the stick spectrum. (b) Vibrational-excitonic resonance for $\omega = 200 \text{ cm}^{-1}$ and vibrational reorganization energy $\lambda_{vib} = 5 \text{ cm}^{-1}$. The upper exciton peak is split into peaks 2a and 2b at 11 654 cm⁻¹ and 11 684 cm⁻¹, respectively. Peaks 2a and 2b are separated by 29 cm⁻¹ due to vibronic coupling between the states $|\beta\rangle |\nu_+^{\beta} = 0\rangle |\nu_-^{\beta} = 0\rangle$ and $|\alpha\rangle|v_{+}^{\alpha}=0\rangle|v_{-}^{\alpha}=1\rangle$. The lower exciton peak 1 lies at 11 469.5 cm⁻¹ (thin gray dashed line). A small peak at 11 669.5 cm⁻¹ with intensity 80× smaller than peak 1 is a FC transition to $|\alpha\rangle |\nu_{+}^{\alpha}=1\rangle |\nu_{-}^{\alpha}=0\rangle$ (second thin gray dashed line). (c) The effect of reducing the site energy gap $\Delta = 122 \text{ cm}^{-1}$ so that the excitonic energy gap of 180 cm⁻¹ is slightly off-resonant with the FC-active vibration of frequency 200 cm⁻¹ on each pigment. The average site energy was adjusted to $(E^A + E^B)/2 = 11$ 563.9 cm⁻¹ at $\lambda_{vib} = 5$ cm⁻¹ in order to keep the lower exciton peak fixed at 11 469.5 cm⁻¹. The upper exciton peak is split into two peaks of unequal intensities located at 11 641 cm⁻¹ and 11 678 cm⁻¹. The weaker split peak is largely $|\alpha\rangle |\nu_+^{\alpha} = 0\rangle |\nu_-^{\alpha} = 1\rangle$ and the stronger has a predominant $|\beta\rangle|v_{+}^{\beta}=0\rangle|v_{-}^{\beta}=0\rangle$ character. The weak FC transition to one quantum of correlated vibration on the lower exciton remains at 11 669.5 cm⁻¹.

spectrum, even at a temperature of 80 K. The differences between the absorption cross sections in the upper and middle panels are slight: the transition to the upper exciton

loses some peak intensity and gains some intensity in the high frequency tail. The spectrum could be made to fit a purely electronic exciton Hamiltonian with site-specific displacements.

To understand the stick spectrum of the simplest case of a dimer with one identical FC-active mode per pigment described above, the delocalized vibrational basis kets $|v_{+}^{X}\rangle|v_{-}^{X}\rangle$ are critical (the right superscript $X=G, \alpha, \beta$ indicates the diabatic electronic state for which the ket is a vibrational eigenstate). Only a quantum of excitation along the anti-correlated vibrational coordinate \hat{q}_{-} on exciton $|\alpha\rangle$ is coupled to the higher energy exciton $|\beta\rangle$. For the stick spectrum (shown in black), the transition to the lower energy exciton has an essentially unmodified $|G\rangle |v_{\perp}^G = 0\rangle |v_{\perp}^G = 0\rangle$ to $|\alpha\rangle |v_+^{\alpha} = 0\rangle |v_-^{\alpha} = 0\rangle$ band origin (peak 1). The higher energy peak is split by 29 cm⁻¹ into two lines (2a and 2b) with nearly equal intensity due to vibronic coupling between the states $|\beta\rangle|v_+^{\beta}=0\rangle|v_-^{\beta}=0\rangle$ and $|\alpha\rangle|v_+^{\alpha}=0\rangle|v_-^{\alpha}=1\rangle$ in Eq. (5). For a purely electronically coupled dimer (vibrational reorganization energy $\lambda = 0 \text{ cm}^{-1}$), the excitonic state $|\beta\rangle|v_+^\beta=0\rangle|v_-^\beta=0\rangle$ has all the intensity (upper panel of Fig. 2). In the presence of FC vibrational displacement upon electronic excitation, this intensity is partially borrowed by the isoenergetic basis state $|\alpha\rangle |v_{+}^{\alpha}=0\rangle |v_{-}^{\alpha}=1\rangle$. This splitting slightly weakens the peak absorption cross section around the upper excitonic transition.

A small peak (coincident with the thin gray dashed line) between the peaks 2a and 2b arises from a transition to the state $|\alpha\rangle |v_+^{\alpha}=1\rangle |v_-^{\alpha}=0\rangle$, with a quantum of excitation along the correlated vibrational coordinate \hat{q}_+ . Since this state does not borrow intensity from the isoenergetic basis state $|\beta\rangle |\nu_{+}^{\beta} = 0\rangle |\nu_{-}^{\beta} = 0\rangle$, a weak $\Delta v_{+} = \pm 1$ FC factor renders transition strength from the ground electronic and vibrational state $|G\rangle |v_+^G = 0\rangle |v_-^G = 0\rangle$ to the state $|\alpha\rangle |v_+^\alpha = 1\rangle |v_-^\alpha = 0\rangle$ $80 \times$ less than the strength for peak 1, as predicted by Eq. (9a). This pattern of two strong transitions that share intensity through vibrational-electronic coupling and one weak transition that is reflective of the intrinsic Franck-Condon factors (with precisely half the Huang-Rhys factor of the isolated pigment) is a direct manifestation of the role of vibrational delocalization in energy transfer coupling treated in Secs. II B and II C. This pattern of intensities appears difficult to understand on the basis of equal coupling to vibrations localized on the donor and acceptor.

With vibrational-electronic resonance, this mixing gives rise to mixed vibrational-electronic eigenvectors with electronic character strongly dependent on the anti-correlated vibrational coordinate.² Thus, transition dipoles from the ground to the excited state of the dimer acquire a strong nuclear coordinate dependence. The Condon approximation, which assumes the electronic transition dipole is independent of vibrational coordinates, breaks down along the anti-correlated vibrational coordinate. Using a Condon approximation⁴⁸ in such a scenario neglects these effects. Such vibrational-electronic mixing has also been shown² to give rise to an "unavoidable nested funnel" on the excited state that allows non-adiabatic energy transfer between the excited states and leads to enhanced Raman excitation of the anti-correlated

vibrational wavepackets on the ground electronic state of the

Higher FC progressions involving transitions from the ground state $|G\rangle |v_+^G = 0\rangle |v_-^G = 0\rangle$ to higher lying vibrational-electronic states with mixed $|\alpha\rangle|v_+^{\alpha}=0\rangle|v_-^{\alpha}=2\rangle$ and $|\beta\rangle |v_+^{\beta} = 0\rangle |v_-^{\beta} = 1\rangle$ character are weak due to a $\Delta v_{-} = \pm 1$ FC factor and lead to very weak peaks in the frequency range 11 850–11 890 cm⁻¹ with intensities \sim 180× less than peak 1. These underlie the intensity gained in the high frequency tail of the absorption cross section. There are also weak hot band transitions from $|G\rangle |v_+^G = 0\rangle |v_-^G = 1\rangle$ to the resonant pair $|\alpha\rangle |\nu_+^{\alpha} = 0\rangle |\nu_-^{\alpha} = 1\rangle$ and $|\beta\rangle |\nu_+^{\beta} = 0\rangle |\nu_-^{\beta} = 0\rangle$ near the band origin peak 1. Similarly, a weak hot band transition from $|G\rangle|v_+^G=1\rangle|v_-^G=0\rangle$ to $|\alpha\rangle|v_+^\alpha=1\rangle|v_-^\alpha=0\rangle$ is also present near peak 1. These hot band transitions derive their strength from $\Delta v_{-} = 0$ and $\Delta v_{+} = 0$ FC factors but are weak because only ~5% of the total ground state population is in the v = 1 levels of the electronic ground state at T = 80 K.

In antenna proteins, there is a distribution of pigment electronic excitation energies and thus a distribution of energy gaps between pigments ($\sigma_{\Delta} = 34 \text{ cm}^{-1}$ was used in Ref. 2). The lower panel of Fig. 2 shows how the stick spectrum and absorption cross section are modified with a different excitonic energy gap. The pigment excitation energies are chosen so that the transition to the lower exciton has the same energy as in the other panels, but the excitonic energy gap is reduced to 180 cm⁻¹ while the vibrational frequency is kept constant at 200 cm⁻¹. Although the underlying model includes the vibrational-excitonic coupling reflected in the stick spectrum, the reduction in upper exciton energy red-shifts the peak absorption cross section for the transition to the "upper exciton" by ~20 cm⁻¹, as expected for a purely electronic model.

Compared to the middle panel, the lower panel shows that level shifts and intensity borrowing are significantly reduced in the stick spectrum. The red-shifted transition to the nominal upper exciton retains over 3/4 of the purely electronic dipole strength shown in the upper panel. Although the transition energies to the lower excitons are precisely coincident (by construction) in the middle and lower panels, the intensity borrowing transition to the state which nominally has one quantum of anti-correlated vibration on the lower exciton is red-shifted in the lower panel because it has a smaller blue-shift from offresonant vibronic coupling. The weak Franck-Condon transition to the state with one quantum of correlated vibration on the lower exciton remains precisely coincident between middle and lower panels (see thin gray dashed line) with exactly the same dipole strength. These observations about the effects of inhomogeneity have implications for hole-burning spectroscopy (see Sec. IV).

Figure 3 shows the line strengths, which indicate vibrational-electronic mixing between the second and the third state in Eq. (5), as a function of vibrational frequency for a fixed excitonic energy gap of 200 cm⁻¹. Unlike the variation in 2D cross-peak oscillation amplitude in Fig. S2 of Ref. 2, there is no ensemble average over an inhomogeneous distribution of excitonic energy gaps; Fig. 3 shows the

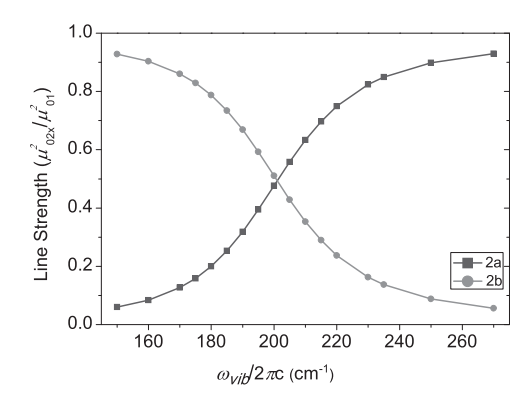


FIG. 3. The line strengths for peaks 2a and 2b in Fig. 2(b) as a function of vibrational frequency for $\Delta^{EX} = 200 \text{ cm}^{-1}$. At the resonant vibrational frequency of 200 cm⁻¹, the two split peaks have nearly equal line strengths.

narrower energetic range for vibrational-excitonic mixing through one vibration within a single antenna. Also, the vibrational displacement d is fixed as vibrational frequency is varied in Fig. 3 (the vibrational reorganization energy λ was fixed in Fig. S2 of Ref. 2). The amplitudes of the split peaks are nearly equal at diabatic vibrational-excitonic resonance;⁴⁹ that is, the intensity borrowing is maximum near $\omega_{vib}/2\pi c = 200 \text{ cm}^{-1}$, with a single dominant excitonic peak for much lower or much higher vibrational frequencies. The slight shift off precise diabatic resonance arises through interference from the weak FC overlap for $\langle v_-^G = 0 | v_-^\alpha = 1 \rangle$. Based on the vibrational-excitonic energy gaps that generate peak strengths with a 1:2 (or 2:1) ratio, a resonance full-width at half maximum (FWHM) of 23 cm⁻¹ is estimated.

The width of such a vibrational-electronic resonance is dictated by the dimensionless FC displacement d, the pigment energy gap Δ , and the electronic coupling J. One can roughly estimate the width of the resonance from the truncated diabatic excitonic Hamiltonian in Eq. (5) [and more precisely from Eq. (34) of Paper I¹¹]. The two coupled pigmentlocalized electronic states have a diabatic excitonic mixing angle of $2\theta_d = \arctan(2J/\Delta) = \arctan(2.66/150) = 0.72$ rad so that, for a vibrational frequency of $\omega/2\pi c = 200 \text{ cm}^{-1}$, the off-diagonal vibrational-excitonic coupling in Eq. (5) is $[\omega d\sin(2\theta_d)/2]/2\pi c = 14 \text{ cm}^{-1}$. The dark state reaches a 1:2 intensity ratio at vibrational-excitonic mixing angles $2\theta_{VE}$ = $\arctan[\omega d \sin(2\theta_d)/(\Delta^{EX} - \omega)]$ that satisfy $\sin^2(\theta_{VE}) = 1/3$. Ignoring the vibrational frequency dependence of the coupling, this would occur at vibrational-excitonic energy gaps (Δ^{EX} $-\omega$) of about ± 10 cm⁻¹. Figure 2 shows that this rough estimate is reasonably accurate and indicates that the truncated Hamiltonian can be quantitatively useful for the dimensionless displacements d found in low frequency bacteriochlorophyll vibrations. A different choice of Coulombic coupling J would change the width of the resonance, as would a different vibrational reorganization energy λ . The finite width of the resonance shows that one must consider how additional FC-active modes lying close to the excitonic energy gap contribute to vibrational-electronic mixing. The assessment of the resonance width is different for cross-peak oscillations in 2D spectroscopy, for which a wider range can be determined from Fig. 2 (see Paper III).⁵⁰

B. Dimer with two FC-active modes per pigment

Fluorescence line-narrowing (see Fig. 5 of Refs. 28, 34, and 36) and resonance Raman studies on the BChl a chromophore (see Fig. 1 of Ref. 35 and Fig. 8 of Ref. 51) that were conducted independently of the 2D experiments on FMO have revealed a broad feature with a solvent dependent structure³⁶ around the 160–200 cm⁻¹ vibrational frequency range. This points to closely spaced FC-active modes in the BChl a chromophore. Features near 161 cm⁻¹ and 195 cm⁻¹ are consistently reported and have been assigned, based on isotopic substitution, to vibrations with highly mixed in-plane deformations of substituent groups, and highly mixed magnesium doming, macrocycle deformation, and substituent group motions, respectively.⁵¹ Four sharper vibrational features at 167 cm⁻¹, 180 cm⁻¹, 191 cm⁻¹, and 202 cm⁻¹, superposed on top of the broad pedestal, have been reported for FMO in Ref. 28 and very similar frequencies have been reported in BChl a films.⁵¹ It is not clear that each feature represents a transition to a single FC active vibrational eigenstate—it could be that each peak represents a FC bright mode coupled to more than one vibrational eigenstate.⁵² All the vibrational frequencies mentioned above have weak reorganization energies and lie close to excitonic energy gaps in the FMO antenna. Calculations²⁵ suggest that additional modes can be enhanced by vibrational-excitonic resonance in fluorescence line narrowing.

It is clear from Fig. 3 that, even if these Raman/fluore-scence peaks do not represent vibrational eigenstates, more than one Franck-Condon bright vibrational state lies within the energetic range of the vibrational-excitonic coupling. To study the effects of nearby FC-active vibrational modes on the dynamics, the case of two FC-active modes on each pigment is treated here under the assumption that the corresponding frequencies and positive FC displacements on each pigment are identical. From Eq. (33) of Paper I, ¹¹ the generalized tuning vector dot product is $\mathbf{g}_d^{A-B} \cdot \hat{\mathbf{q}} = -\sqrt{2}\omega_1 d_1 \hat{q}_{1-} - \sqrt{2}\omega_2 d_2 \hat{q}_{2-}$, where the subscripts 1 and 2 correspond to the two intramolecular FC active vibrational modes. The total single exciton Hamiltonians \hat{H}_1 is a sum of the correlated and interaction Hamiltonians in Eqs. (32) and (34) of Paper I, respectively. ¹¹

The second FC-active vibration has frequency 180 cm⁻¹ and reorganization energy $\lambda_{vib} = 5 \text{ cm}^{-1}$ on each pigment. The reorganization energy for line broadening now becomes $\lambda_{eff} = 25 \text{ cm}^{-1}$ (instead of 30 cm⁻¹), such that the total reorganization energy is constant at 35 cm⁻¹. All the other parameters are the same as used for the one-mode dimer case (Sec. III A).

Figure 4 shows the stick spectrum and absorption cross section. Due to the near-resonant mode at 180 cm⁻¹, the three isoenergetic states in Eq. (6) are accompanied by states with a quantum of excitation along the correlated and anti-correlated coordinates for the near-resonant mode. The stick spectrum shows that for a dimer with two near resonant FC active modes per pigment, the intensity of the transition to the upper exciton is shared among three strong lines: the upper exciton plus two anti-correlated vibrational states on the lower energy exciton. The 3 lines can have roughly equal intensities depending on the choice of parameters for the two individual FC-active

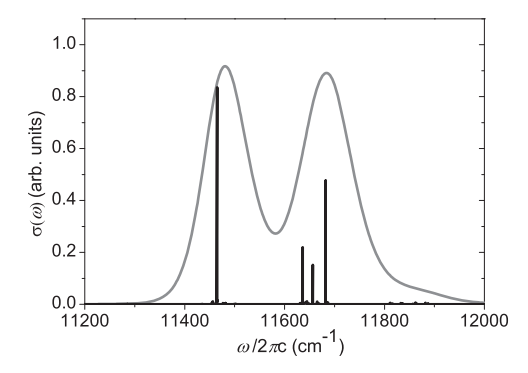


FIG. 4. Absorption cross section for a dimer with 2 FC active vibrational modes per pigment. The average site energy is $(E^A + E^B)/2 = 11\,574~{\rm cm}^{-1}$ and the site energy gap between pigments is $\Delta = 150~{\rm cm}^{-1}$ with coupling $J = 66.14~{\rm cm}^{-1}$ such that the excitonic energy gap is $\Delta^{EX} = 200~{\rm cm}^{-1}$. The vibrational frequencies are $180~{\rm cm}^{-1}$ and $200~{\rm cm}^{-1}$, each with $\lambda_{vib} = 5~{\rm cm}^{-1}$. The remaining line broadening is calculated for a critically damped Brownian oscillator with $70~{\rm cm}^{-1}$ frequency and reorganization energy $\lambda_{eff} = 25~{\rm cm}^{-1}$ at a temperature of T = 80 K. Peaks are normalized relative to peak 2 in Fig. 2(a). The lower exciton lies at $11\,465~{\rm cm}^{-1}$. The upper exciton peak is split into three peaks with different intensities at $11\,636~{\rm cm}^{-1}$, $11\,657~{\rm cm}^{-1}$, and $11\,682~{\rm cm}^{-1}$.

modes. This sharing among three lines for two near-resonant, FC-active vibrational modes per pigment extends the intensity sharing among two peaks with one near-resonant, FC active vibrational mode per pigment. Thus, with n FC-active vibrational modes per pigment lying close to the excitonic energy gap, the dipole strength of the upper exciton can be distributed to n dark basis states of excited, anti-correlated vibrational levels on the lower energy exciton, yielding n+1 peaks with bright upper exciton character. Significant redistributions of intensity are not additive.

Very weak peaks between the three split peaks under the higher energy exciton at frequencies 11 645 cm⁻¹ and 11 665 cm⁻¹ correspond to transitions from the ground electronic and vibrational state to the lower energy exciton with one quantum of excitation along the correlated vibrations at 180 cm⁻¹ and 200 cm⁻¹, respectively. These peaks are $\sim 80 \times$ less intense than the lower exciton peak at 11 465 cm⁻¹. $\sim 5\%$ of the total ground state population has one quantum of vibrational excitation at T = 80 K, allowing weak hot bands near the lower exciton.

At 80 K in FMO, the total linewidth of the 0-0 bands and the width of the vibrational-excitonic resonance are such that the nominal higher-exciton band is hardly affected by such mixing and the peak splittings are completely hidden under the broadened line shapes. For a single mode, the subtle effect of the splitting in the underlying stick spectrum was most apparent as a decrease in peak absorption cross section around the transition to the upper exciton (compare upper and middle panels of Fig. 2). For coupling to two modes, the underlying splittings in the upper exciton transition stick spectrum cause both a reduction in peak absorption cross section and a visible broadening in Fig. 4 when compared to the purely electronic model with the same excitonic energy gap in the upper panel of Fig. 2. Such slight effects of splitting on the absorption cross section could be accommodated in a purely electronic model by invoking differences between pigment couplings to the bath.

C. Vibrational-excitonic resonance reassembles a split vibration

The Raman spectrum of BChl a reveals complicated line shapes that are not strongly dependent on temperature.^{35,51} This suggests that FC bright vibrational character is fragmented over a few normal modes. To investigate how such fragmentation (which generates a spectral density of coupled modes when taken to the limit) affects vibrational excitonic resonance, we consider a two-mode model in which a vibrational reorganization energy of $\lambda_{vib} = 5 \text{ cm}^{-1}$ on each pigment is split evenly between two vibrations with slightly different frequencies. Figure 5 shows the results as the frequency of the second vibration is reduced while that of the first is held fixed at 199 cm⁻¹ along with the 200 cm⁻¹ excitonic energy gap. Transitions starting from vibrationally hot states are negligible at 1 K. As expected, the 0-0 transition to the lower exciton is hardly affected, and the stick spectrum with 180 and 199 cm⁻¹ vibrations resembles Fig. 4 (but differs because the summed vibrational reorganization energy for the two modes is half of that in Fig. 4). As the vibrational frequencies approach each other (red to black stick spectra), an interference effect develops and the upper exciton region contains only two lines. It is most interesting that for small splittings, the vibrational-excitonic resonance essentially "reassembles" a single maximally coupled state.

For 198 and 199 cm⁻¹ vibrations on each pigment, the stick spectrum strongly resembles Fig. 2(b), which shows a single 200 cm⁻¹ vibration with the same summed vibrational reorganization energy. Although two vibrations are resonantly coupled, only one extra line is lit up by the vibrational-excitonic resonance. For the same mathematical reasons explained in discussing Eq. (5), this "reassembly" is perfect if the two vibrations have the same frequency. This reassembly of the coupled mode gradually goes away as the split-off vibration leaves the range of the vibrational-excitonic resonance. Re-interpreting the parameters, this reassembly of the coupled modes also illustrates how a single anti-correlated mode can be fashioned out of localized modes on the donor and acceptor, even when their vibrational frequencies are slightly different. For the original interpretation, with two localized modes on each pigment, a total of 4 coupled vibrations combine such that only one acceptor eigenstate is lit up by the donor exciton. The supplementary material shows similar effects on spectra for models of vibrational splitting on one pigment through coupling to environmental modes. This suggests that vibrational-excitonic resonance cannot only reassemble splittings but may "defragment" a fragmented vibrational state. The circumstances which allow excitonic resonance defragmentation of a fragmented vibrational state require further

D. Dimer with one FC-active mode per pigment and a global environmental mode

We now consider the effect of one environmental vibrational mode belonging to the protein that surrounds the pigments along with one FC-active vibrational mode on each pigment. An environmental mode with frequency ω_e will in general experience a displacement in equilibrium

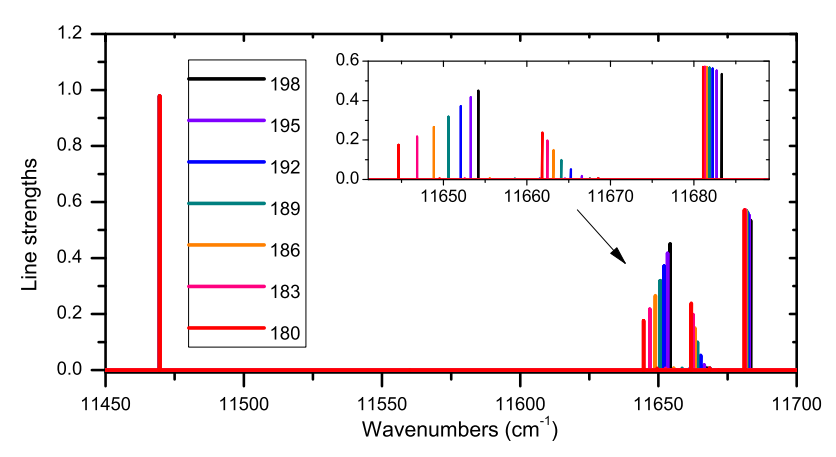


FIG. 5. Absorption stick spectra for a non-degenerate homodimer with a 90° angle between pigment transition dipoles and two FC active vibrational modes per pigment. The average excitation energy is $(E^A + E^B)/2 = 11$ 574 cm⁻¹ and the site energy gap between pigments is $\Delta = 150$ cm⁻¹ with coupling J = 66.14 cm⁻¹ such that the excitonic energy gap is $\Delta^{EX} = 200$ cm⁻¹. The frequency of one FC active vibrational mode is fixed at 199 cm⁻¹, while the other FC active vibrational mode frequency is varied from 198 cm⁻¹ to 180 cm⁻¹. The reorganization energy for each vibrational mode is fixed at $\lambda_{vib} = 2.5$ cm⁻¹ so that the two modes split the vibrational reorganization energy of $\lambda_{vib} = 5$ cm⁻¹, in Fig. 2(b) or 2(c). The spectrum is calculated at a temperature T = 1 K. The intensity of the lower exciton does not change with the frequency of the near-resonant vibrational mode, and its frequency (11 469.5 cm⁻¹) is unperturbed to one decimal place. In general, the transition to the upper exciton splits into three peaks, shown in more detail in the inset. The smallest vibrational frequency difference (black stick spectrum) closely resembles Fig. 2(b), with two dominant peaks replacing the upper exciton peak. The largest vibrational frequency difference (red (black stick spectrum)) resembles Fig. 4, with three peaks splitting the upper exciton intensity. A weak FC transition (~0.6% of the lower exciton peak) to one quantum of correlated 199 cm⁻¹ vibration on the lower exciton occurs at 11 668.5 cm⁻¹ for all models. Equally weak FC transitions to the correlated lower frequency vibration on the lower exciton shift to the red. When both vibrational frequencies are close to each other, the middle anti-correlated black peak has destructive interference that yields less intensity than the FC transition to one quantum of correlated vibration; as a result, it is not seen on the scale of the figure. The lower black peak gains this intensity through constructive interference.

coordinate upon electronic excitation of either pigment, but the displacements d_e^A and d_e^B are not simply related. In general, low-frequency protein modes are anharmonic at physiological temperature⁵³ and the assumption of a harmonic protein mode made here may not describe the dynamics for very long.

With a single mode affecting both pigments unequally (as in the special pair in the bacterial photosynthetic reaction center⁵⁴), the separation into \hat{H}_+ and \hat{H}_- in Eqs. (32) and (34) of Paper I¹¹ (or \hat{H}_{corr} and \hat{H}_{int} , respectively, in Ref. 2) no longer applies and we must revert to Eq. (1) or (2) given here. The environmental mode must be included in the nonadiabatic Hamiltonian but will alter the average pigment excitation energy (like a delocalized intramolecular vibration that is anti-correlated but not anti-symmetric). Apart from the anti-correlated vibrations \hat{q}_{i-} , which tune the relative energy gap between the singly excited states and allow non-adiabatic energy transfer between them, additional contributions from the environmental mode \hat{q}_e in tuning the relative energy gap [Eq. (25) of Paper I¹¹] can affect the non-adiabatic energy transfer between the pigments. Recently⁴⁰, such delocalized environmental vibrational modes in the FMO antenna complex have been implicated in the fast dephasing of coherences and fast energy transfer. When the environmental vibrational mode is symmetric, that is, when the FC displacements on the excited state of the two pigments due to the environmental mode become equal, the contribution of the environmental mode towards the tuning vector \mathbf{g}_d^{A-B} vanishes [Eq. (25) of Paper I¹¹], and energy transfer between the pigments due to the anti-correlated vibrations is not affected. This absence of energy transfer coupling for equal displacements of a common mode was noted by Soules and Duke in 1971,⁵⁵ who also noted the implication that acoustic phonons with wavelengths much longer than the pigment separation play no role in energy transfer.

The calculations here include one environmental mode and the pigment mode with vibrational-excitonic resonance treated in Sec. III A. The low-frequency phonon sideband of BChl a in the FMO complex peaks at around 20 cm⁻¹ and has an integrated Huang-Rhys factor, Senv of 0.3, when measured at a low energy fluorescence excitation wavelength^{28,34} of ~829 nm. The total reorganization energy from the asymmetric phonon sideband is ~11 cm⁻¹. A similarly low environmental Huang-Rhys factor has been reported for BChl a in a lauryldimethylamine N-oxide (LDAO) detergent/water glass.³⁷ Given the distance between pigments, their electronic excitations may be coupled to different protein vibrational modes, but there are no experimental data bearing directly on this point aside from the 2D spectra (for which the roles of pigment and protein vibrations are studied in Paper III).⁵⁰ In the paper by Renger et al., 40 calculated diagonal spectral densities in Fig. 2 and energy gap spectral densities in Fig. 4 suggest that FMO protein modes with frequencies above 20 cm⁻¹ tend to be primarily coupled to one pigment, while lower frequency modes are more likely to be delocalized so that they affect more than one pigment. For exploratory purposes, we choose a displacement for the environmental mode that is maximally different from both correlated and anti-correlated intramolecular pigment vibrations.

Based on the above discussion, in order for the protein environment to affect energy transfer, both excited pigments must be coupled differently to the protein vibrational mode. Here we assume that only the higher energy pigment, B, is coupled to the environmental mode, with a reorganization energy of 3 cm⁻¹. This is about a quarter of the reorganization energy of the lowest energy pigment due to

the environment (as measured with red-edge excitation). The reorganization energy of 3 cm⁻¹ for the *higher* energy pigment due to its coupling to the environment does not contribute towards the total Stokes' shift determined from emission by the *lowest* energy exciton. Only the intramolecular vibrational reorganization energy of 5 cm⁻¹ for the lowest pigment contributes towards the total reorganization energy of 35 cm⁻¹ from Ref. 56 such that the reorganization energy needed for broadening of line shapes remains $\lambda_{eff} = 30 \text{ cm}^{-1}$. All the other parameters are the same as for the one-mode per pigment dimer in Sec. III A.

Figure 6 shows the low temperature (4 K) absorption and emission spectra for the dimer model with one environmental mode 6(a), one pigment vibration 6(b), and a pigment vibration plus an environmental mode 6(c). The model does not include inhomogeneous broadening. The strongly asymmetrical line shapes arise from the quantum mechanical critically damped Brownian oscillator model⁴⁵ used for line broadening, which effectively generates a reasonable line shape for modeling 2D spectra at higher temperature (80 K)² but does not resemble the low temperature line shapes measured through hole-burning and line-narrowing; ^{28,29,36,37,43} the phonon sidebands in such low temperature line shapes require a large number of more weakly coupled, underdamped quantum oscillators. ⁵⁷ The most important features in Fig. 6 are the stick spectra.

Figure 6(a) shows that the environmental mode coupled to pigment B, by itself, adds a vibrational satellite only to the absorption band for the transition to the upper exciton (which has primarily character corresponding to electronic excitation of pigment B). Absorption to the lower exciton is essentially unaffected. The relaxed emission spectrum, which involves exclusively emission from the lower exciton, is also unaffected.

Figure 6(b) shows the 4 K temperature spectra for a pigment vibrational mode alone. The absorption spectrum can be compared to the 80 K absorption spectrum in Fig. 2(b) both show the homogeneous spectrum for a single dimer in the ensemble. The weak hot bands in the 80 K absorption spectrum are absent at 4 K because all transitions originate from the zero point level on the ground electronic state. The absorption spectrum clearly shows the splitting from the strong vibronic interaction between the zero-point level on the upper exciton and one quantum of anti-correlated vibration on the lower exciton. The stick spectrum again shows an unperturbed, very weak Franck-Condon transition to one quantum of correlated vibration on the lower exciton, but this is obscured in the absorption spectrum. The absorption spectrum also shows very weak peaks about 200 cm⁻¹ blue of the upper exciton (about 150× weaker than the lower exciton). These involve a $\Delta v_{+} = 1$ transition to $|\beta\rangle |v_{+} = 1\rangle |v_{-} = 0\rangle |v_{E} = 0\rangle$ and a transition to the resonant pair $|\beta\rangle |\nu_+ = 0\rangle |\nu_- = 1\rangle |\nu_E = 0\rangle$ and $|\alpha\rangle |\nu_+ = 0\rangle |\nu_- = 2\rangle |\nu_E = 0\rangle$, which share a small $\Delta\nu_- = 1$ FC factor.

Figure 6(c) shows the combined effect of the environmental and pigment modes in Figs. 6(a) and 6(b). The splitting of the absorption transition to the zero-point level on the mixed (upper exciton)/(one quantum of anti-correlated vibration on the lower exciton) states is quite similar to that in Fig. 6(b). However, the intensity of the absorption transition

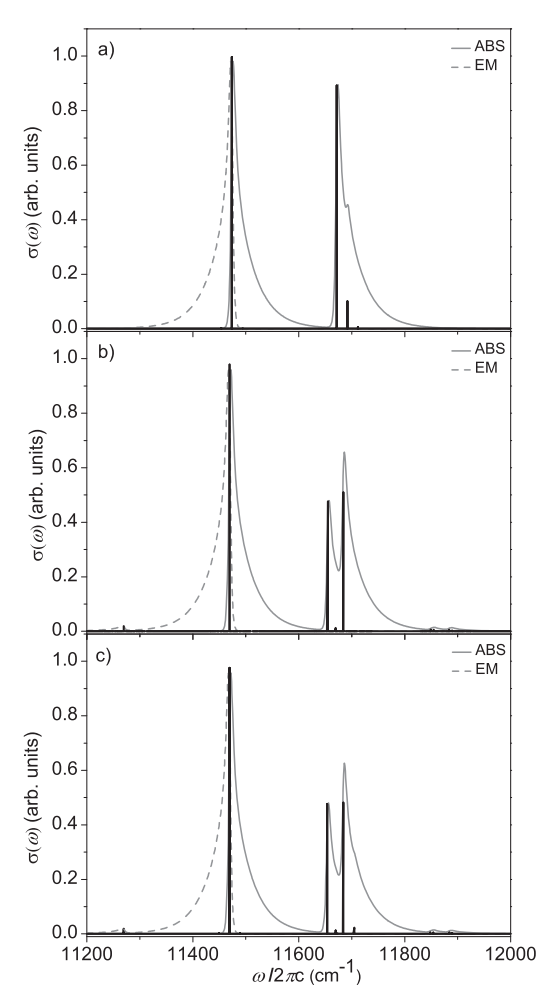


FIG. 6. Absorption (solid gray) and emission (dashed gray) cross sections for a non-degenerate homodimer with a 90° angle between pigment transition dipoles, one 200 cm⁻¹ frequency FC active vibration per pigment, and a global environmental mode at a temperature of T = 4 K. The average site energy is $(E^A + E^B)/2 = 11 574 \text{ cm}^{-1}$ and the site energy gap between pigments is $\Delta = 150 \text{ cm}^{-1}$ with coupling $J = 66.14 \text{ cm}^{-1}$ such that the excitonic energy gap is $\Delta^{EX} = 200 \text{ cm}^{-1}$. The stick spectra are normalized relative to the purely electronic dimer model in Fig. 2(a). The critically damped Brownian oscillator line shapes have a frequency of 70 cm⁻¹ and $\lambda_{eff} = 30$ cm⁻¹. (a) Pigment B is coupled to an environmental mode with reorganization energy $\lambda_{env} = 3 \text{ cm}^{-1}$. There is no coupling to pigment vibrations. The lower exciton transition is located at 11 474 cm⁻¹ in both absorption and emission. The upper exciton absorption shows a short progression in the environmental mode. The 0-0 transition at 11 672 cm⁻¹ is ~200 cm⁻¹ above the lower exciton peak and is accompanied by a ~10× weaker peak at 11 692 cm⁻¹ with one quantum of excitation in the 20 cm⁻¹ environmental mode. (b) Absorption and emission spectra for a dimer model with one intramolecular vibrational mode per pigment ($\lambda_{vib} = 5 \text{ cm}^{-1}$) and no coupling to environmental modes [like that in Fig. 2(b)]. The absorption spectrum is described in Fig. 2(b) and has a 0-0 transition to the lower exciton at 11 470 cm⁻¹. The emission spectrum contains weak overlapping transitions to $v^G = 1$ states at 11 270 cm⁻¹. Their summed intensity is $0.78 \times$ that for the $\Delta v = 1$ emission in a monomer. (c) The absorption and emission spectra for a dimer model with one vibration per pigment and an environmental mode coupled to the higher energy pigment (B). The upper exciton peak in absorption is split into three peaks with two having nearly equal intensities at 11 654 cm⁻¹ and 11 684 cm⁻¹, respectively. As in panel (b), these peaks are separated by 29 cm⁻¹ and surround a FC transition to $|\alpha\rangle |\nu_+ = 1\rangle |\nu_- = 0\rangle |\nu_E = 0\rangle$ at 11 670 cm⁻¹. The ~40× weaker peak at 11 705 cm⁻¹ is about 20 cm⁻¹ above from the upper split peak at 11 684 cm⁻¹ and adds one quantum of excitation along the environmental

to the upper exciton with one quantum of environmental vibration is significantly reduced relative to these split transitions, indicating non-additive interactions between environmental and anti-correlated pigment modes, as suggested by the discussion in Sec. III C of Paper I.¹¹ Other features of the absorption and emission spectra appear to be additive, misleadingly suggesting rough adiabatic separability.

E. Vibrational satellites in emission

The relaxed emission spectrum in Fig. 6(b) is thermally equilibrated at 4 K and contains emission exclusively from the zero point level of the lower exciton. It is dominated by strong 0-0 emission without any change in vibrational quantum numbers but also contains red-shifted emission from the zero-point level on the lower exciton to one quantum of pigment vibration in the ground-electronic state. This emission line is a sum of perfectly overlapping transitions that terminate on two degenerate vibrational levels, with one quantum in the correlated or anti-correlated vibration, respectively. Relative to the 0-0 transition, the intensity of the weak Franck-Condon emission to the state with one quantum of correlated vibration is unaffected by exciton delocalization caused by the energy transfer coupling, as expected from the adiabatic separability of the correlated vibration. In other words, Eq. (9a) applies and the Huang-Rhys factor for the correlated vibration in the dimer is 1/2 that of the localized vibration in a monomer.

Interestingly, the intensity of the emission transition to the anti-correlated vibrational state is also accurately calculated by the Condon approximation. As can be seen by comparing Eqs. (1) and (2), the excitonic coupling reduces the electronically diagonal but vibrationally off-diagonal effect of the anti-correlated vibrations by a factor of $\cos(2\theta_d)$, where θ_d is the mixing angle for the excitonic states arising from the energy transfer coupling. This reduces the equilibrium displacement of the anti-correlated vibration by the same factor, which reduces the Huang-Rhys ratio of FC vibrational overlap factors for emission from the zero-point level of the excited electronic state to the electronic ground state with one quantum of excitation in the anti-correlated vibration by a factor of $\cos^2(2\theta_d)$. In other words, Eq. (9b) applies and the Huang-Rhys factor for the correlated vibration in the dimer is $(1/2)\cos^2(2\theta_d)$ that of the localized vibration in a monomer. Relative to the 0-0 transition, the sum of the intensities for Franck-Condon allowed emission to both $v^G = 1$ levels in the dimer is $(1/2) + (1/2)\cos^2(2\theta_d) \approx 0.78$ of the relative intensity in the monomer. The sum of the two dimer (0-1) emission strengths $I_{dimer}(0-1)$ is $S_{monomer}[(1/2) + (1/2)\cos^2(\theta_d)]$ times the dimer (0-0) emission strength I_{dimer} (0-0), where $S_{monomer}$ = $I_{monomer}(0-1)/I_{monomer}(0-0)$ is the monomer Huang-Rhys factor [see Eq. (10)].

This match between Franck-Condon and exact non-adiabatic intensities indicates that the zero-point level of the lowest exciton is well described by the adiabatic approximation even though no other levels of the dimer are. Resonant vibronic coupling lights up the anti-correlated pigment vibration so that it is almost as strong as a purely electronic transition in the absorption spectrum but suppresses the anti-correlated pigment vibration to less than half the corresponding Franck-Condon intensity of the isolated pigment in the relaxed emission spectrum. Excitonic coupling is known to

artificially suppress vibrational satellite intensity in fluorescence line narrowing experiments, ²⁵ the new insight here is that only the anti-correlated vibration's satellite intensity is suppressed.

IV. DISCUSSION

The model presented in Ref. 2 and developed in Paper I¹¹ depends on three key factors: the small displacements between equilibrium geometries of the ground and first excited states of pigments; protein fine-tuning of the excitation energies for pigments in different protein sites such that their excitonic energy gap resonates with a vibrational frequency having a small geometry displacement; and a protein structure that holds the pigments in an electronically coupled geometry. Together, the magnitude of this displacement and the magnitude of the coupling set an accuracy requirement for protein fine-tuning of the energy gap between pigments that will drive non-adiabatic vibrational-exciton resonance. When the donor and acceptor pigments have similar vibrational frequencies, both vibrations are coupled in an anti-correlated fashion and their anti-correlated motion acts to increase the effective energetic range of the resonant vibrational-excitonic coupling; anti-correlated vibrations double the energetic coupling range for identical vibrations on donor and acceptor. Since the range of the resonance found here for a simple model of a vibrational excitonic resonance in FMO is similar to the inhomogeneity in an FMO excitonic donor-acceptor energy gap as measured through the pump-probe polarization anisotropy decay by Savikhin, Buck, and Struve, 41 it seems that this resonance range doubling by anti-correlated vibrations is likely to play an important role in the energy transfer process on the excited state of FMO and other antennas.

Questions about how fluctuations and damping compete with the resonances that cause vibrational delocalization remain. This competition has been investigated with the hierarchical equations of motion⁵⁸ and a surrogate Hamiltonian approach.⁵⁹ These studies reported temperature dependent (partial) suppression of specific resonance effects. Thermal excitations increase both damping fluctuations and the nonadiabatic coupling (see Fig. 1). As noted in the discussion of Fig. 6, the model used in Refs. 11 and 58 lumps underdamped vibrations in with overdamped low frequency modes so that a single overdamped mode can be used to approximate 2D peakshape broadening at temperatures around 77 K. Aside from the differences in damping, underdamped and overdamped vibrations play different roles in vibronic decoherence, which is slower than electronic decoherence and is the relevant decoherence for energy transfer through vibrational-excitonic resonance.¹¹ The above considerations suggest that additional study of the interaction between vibrational-excitonic resonances and other vibrations is needed.

For electronically excited states of an antenna, systematic vibrational-excitonic resonance dramatically alters every excitonic level except for the final acceptor, which is still quantitatively perturbed. In linear spectroscopy, even the strongest vibrational-excitonic resonance effects can be qualitatively masked by line broadening. Incoherent energy transfer can also cause the effective Huang-Rhys factors for

the environmental phonon sideband to increase with excitation energy. 28,29,43 This raises the question of how to determine vibration-excitonic resonance model parameters from experiments. In emission from FMO, it has been found that the effective Huang-Rhys factors are depressed below those of the isolated pigment by excitonic coupling.²⁵ This accords with the results found here and supports use of the isolated pigment parameters as a starting point for intramolecular vibrations. The question of coupling to environmental modes is more challenging because site-to-site variations can be obscured by vibrational-excitonic resonance or energy transfer and the interactions are not additive. The non-additive suppression of the weakly coupled environmental mode by a weakly coupled vibration found in Fig. 6 is opposite the non-additive enhancement of a weakly coupled vibration by a strongly coupled vibration reported by Zhao and Spano.⁶⁰ Protein modifications of pigment electronic structure 40,61 are likely connected to factors such as Mg coordination and to be smaller than the effective site-to-site variations retrieved from experiment.

A. Chlorophylls and nested funnels in photosynthesis

Chlorophylls, which are responsible for most of the light harvesting on our planet, 62 have a planar (or near-planar), fully conjugated macrocyclic ring of π bonds. The strongly allowed Q_{ν} transition from the ground electronic state to the first excited singlet state has fully delocalized π - π * character. 63 For the aromatic ring in bacteriochlorophyll a, the excitation of one π electron (out of 54) from a bonding orbital to an anti-bonding orbital causes less than a 4% change in average bond order, with correspondingly small changes in equilibrium bond lengths. The main effect of electronic π - π * excitation is a very slight expansion of a fairly rigid ring. Even in 4-fold symmetric porphine, ⁶⁴ this expansion is divided among several normal modes of vibration, and displacements of vibrational equilibrium upon electronic π – π * excitation are spread over more vibrations by the lower symmetry of the chlorophylls⁶⁵ (which would have C_s point-group symmetry if planar).

Experimental determinations of vibrational displacements upon electronic excitation in the Q_v band using the Franck-Condon principle consistently indicate dimensionless displacements d of less than $0.3.^{28,34,37}$ Since dimensionless displacements of ± 1 correspond to the classical turning points at the zero-point energy, the change in equilibrium coordinate for each vibration is much less than the width of the vibrational eigenfunction for the zero-point level. This implies that the typical schematic showing potential curves for energy transfer or charge transfer that are displaced by the width of the potential at the zero-point level (or more) is qualitatively misleading the curves are so slightly displaced that they are nested, intersecting only *above* the first few levels. For electron transfer, such potentials would be in the Marcus inverted region,⁶⁶ but the small energy gaps, nearly identical shapes for the potential curves, and small displacements are far from the usual qualitative picture of radiationless transitions in internal conversion. As a result of these small displacements, the resonant vibronic matrix element is hardly attenuated in the usual waythe product of Franck-Condon overlap integrals for which all other modes conserve their quantum numbers is near unity (see Paper I). 11

The formal similarities between theories for charge transfer and energy transfer are well known, 67 suggesting questions about whether mechanisms similar to that discussed here could be involved in charge transfer. For photosynthetic charge transfer between chlorophylls, the same argument given above for π – π * excitation indicates that intramolecular vibrations have small equilibrium displacements upon oxidation or reduction (loss of one bonding π electron or gain of a single anti-bonding π^* electron out of 54 in *BChl a*). For the chlorophyll a macrocycle, corresponding equilibrium bond lengths calculated for the cation, neutral, and anion all differ by less than 3%, ⁶⁸ and calculated Huang-Rhys factors ⁶⁹ indicate vibrational displacements of less than 1 upon oxidation or reduction. π and π^* orbitals have similar charge distributions so that optical excitation (hence energy transfer) is coupled to the surrounding protein environment through smaller changes in charge density on peripheral substituents.⁷⁰ Gain or loss of a charge is more strongly coupled to the protein environment, but this is tempered by charge delocalization over the conjugated ring. The change in bond displacements within each intramolecular vibrational normal mode upon oxidation or reduction⁷¹ appears to be a more significant difference between charge transfer and energy transfer. These observations suggest that a modified vibrationally resonant nested funnel mechanism, with slightly different donor and acceptor vibrational frequencies, could be involved in the primary charge transfer of photosynthesis. In this connection, further investigation of 2D signatures reported in the photosystem II reaction center of plants^{72,73} could be quite illuminating. In Sec. IV B, the electron transfer model of Won and Friesner^{5,6} will be compared to the energy transfer model developed here.

B. Absorption and hole burning spectra

The absorption spectra in Figs. 2, 4, and 5 show mixed vibrational-electronic transitions in which nominally vibrational states acquire transition strengths comparable to purely electronic transitions through resonantly enhanced coupling. Under these conditions, perturbation theory fails and resonant vibrations must be treated on an equal footing with the coupled electronic states. As can be seen from Fig. 3, the resonance condition requires a near match between one quantum of vibrational energy and the electronic energy gap between two excitons (not the electronic energy gap between two pigments).

Although all of the stick spectra shown here have sharp lines from the vibrational-excitonic resonance, such sharp lines in cryogenic hole burning or fluorescence line-narrowing spectra would be washed out by anti-correlated line broadening. Although anti-correlated line broadening is not included in the stick spectra shown here, a comparison between spectra with different energy gaps between single-exciton states allows its effects to be understood on a line by line basis. Figures 2(b) and 2(c) show absorption spectra with the same 0-0 transition energy for the lowest exciton, but different energy gaps between single exciton states. In a hole burning experiment, both of these spectra have the same frequency for the

zero-phonon transition to the lowest exciton and would be hole-burned together at that frequency. However, the zerophonon lines for satellite transitions to the coupled zero-point level in the mixed (upper exciton)/(one quantum of anticorrelated vibration on the lower exciton) states have different frequencies in the two spectra. An inhomogeneous distribution of energy gaps between single-exciton states would correspondingly broaden these satellite transitions (the anisotropy experiments at 19 K indicate broadening over a standard deviation of ~34 cm⁻¹ for two excitons in FMO). In agreement with this expectation, we are not aware of any report that holeburning the lowest exciton gives rise to satellites from higher excitons in a photosynthetic protein (a fairly recent review discusses broad holes and anti-holes from burning higher excitons as an effect of hole-burning individual pigments⁷⁴). Interestingly, the transition to the lower exciton state with one quantum of correlated vibration occurs at exactly the same frequency for the spectra shown in both Figs. 2(b) and 2(c); averaging over the inhomogeneous distribution of energy gaps between single-exciton states could give a sharp vibrational satellite reflecting the Franck-Condon factor for the v = 0 to v = 1 transition of the correlated vibration. However, these appear to be below the noise level of antenna hole-burning spectra^{37,75,76} and may be further obscured by the hole burning mechanism.⁷⁴ Reference 76 has reported an unexplained 77 satellite hole 74 cm⁻¹ below the hole-burning frequency in the lowest exciton of FMO. This is below any known exciton and might arise from a $v_+ = 0$ satellite hole after burning $v_+ = 1$; the frequency is close to a ~68 cm⁻¹ ground state vibrational frequency in FMO,²⁸ the hole width is close to *BChl a* resonance Raman linewidths, 35 and the vibrational energy might be low enough to avoid triggering the slight protein conformational rearrangements hypothesized⁷⁸ to explain the typical lack of narrow holes on the high frequency side of the lowest exciton.

This proposed mechanism for lowering the intensity of the vibrational satellites in hole-burning below the typical noise level through transitions to delocalized correlated vibrations has implications for determining the Franck-Condon displacements in antenna complexes if such holes could be observed. For a dimer model with equal Franck-Condon displacements for two identical pigments, comparison between Eqs. (32) and (1) of Paper I¹¹ shows that the Franck-Condon displacement of the delocalized correlated vibration on each exciton state is a factor of $\sqrt{2}$ smaller than the Franck-Condon displacement of the localized vibration on an isolated pigment. This reduces the Huang-Rhys factor $|\langle v_{+}^{G} = 0 | v_{+}^{\alpha} = 1 \rangle|^{2} / |\langle v_{+}^{G} = 0 | v_{+}^{\alpha} = 0 \rangle|^{2}$ for the correlated vibration to half of that of the isolated pigment. This result is independent of the excitonic coupling, but as the excitonic coupling vanishes, the anti-correlated vibration becomes less mixed with the upper exciton, hence less washed out by anti-correlated electronic inhomogeneity, and ultimately becomes a sharp vibrational satellite with the missing half of the intensity.

In the dimer model, non-adiabatic interactions reduce the vibrational satellite intensity in hole-burning by 50%, which is more than adiabatic interactions reduce the total 0-1 vibrational band intensity in relaxed emission from the lowest exciton at cryogenic temperatures. The summed

intensity for emission transitions from $|\alpha\rangle |v_+^{\alpha} = 0\rangle |v_-^{\alpha} = 0\rangle$ to $|G\rangle |v_+^G = 1\rangle |v_-^G = 0\rangle$ and to $|G\rangle |v_+^G = 0\rangle |v_-^G = 1\rangle$ is reduced by 22% for this model [see discussion of Fig. 6(b) in Sec. III E]. Vibrational satellite intensities in the dimer depend strongly on the electronic coupling and energy gap. For this reason, we have taken the Franck-Condon displacements from experiments on isolated pigments, which should report larger Franck-Condon displacements than fluorescence linenarrowing experiments on antenna complexes. This influence of excitonic coupling on the vibrational band intensities in the complex is also why Won and Friesner⁶ used monomeric pigment parameters to develop their Hamiltonian for the primary electron transfer in bacterial reaction centers. The weaker interactions here allow a zero-phonon line for the lower exciton and are quite distinct from the much larger broadening of both upper and lower exciton holes through stronger, not necessarily resonant, charge transfer interactions in the Hamiltonians developed by Friesner and co-workers^{6,7} for the primary electron transfer in bacterial photosynthetic reaction centers.

C. Emission and stimulated Raman spectra

Although the 2D spectra calculated for the dimer model by Tiwari et al. show a resonant enhancement of the anticorrelated vibration on the ground electronic state, the calculations here show that there is no resonant enhancement of vibration in relaxed emission from the lowest exciton. As explained by Tiwari et al., the enhancement in 2D spectra occurs through a stimulated Raman process involving the mixed states arising from the resonant coupling between the upper exciton and the anti-correlated vibration; this resonant coupling enhancement "lights up" the anti-correlated vibration so that it has much more than the Franck-Condon amplitude. By contrast, emission from the zero-point level of the lowest exciton does not involve the resonantly coupled levels, is well described by the adiabatic approximation, and consequently shows only the Franck-Condon intensity for vibrational excitation, which is slightly less than the Franck-Condon intensity for vibrational excitation in the isolated pigment.

Interestingly, if the isolated pigments obey the Condon approximation, the non-adiabatic stimulated Raman pathways cancel in integrated pump-probe transients in the fully impulsive limit of delta function pulses, leaving only electronic beats on the excited state. We have computationally verified this "witness" experiment prediction by Aspuru-Guzik and coworkers⁷⁹ for the dimer model. A similar cancellation had previously been noted for non-adiabatically coupled vibrations in square symmetric molecules.²³ Both of these impulsive cancellations for non-adiabatic dynamics arise from the well-understood impulsive cancellation of Raman vibrational wavepacket excitation for isolated molecules in the Condon approximation; 80,81 as in that case, such cancellation likely requires pulses with spectra much broader than the electronic absorption bands from all excitonically coupled transitions. A practical difficulty with the "witness" experiment is that the Q_{y} transition of the isolated BChl a pigment does not obey the Condon approximation ^{36,82} so that vibrational wavepacket signals could survive in the impulsive limit.

References 72, 73, and 83 report oscillation frequencies in 2D spectra of excitonically coupled systems that are below the noise in resonance Raman spectra. In each case, the lack of a corresponding Raman peak has been used to argue that the non-corresponding oscillation originates from electronic coherence or mixed vibrational-electronic coherence⁷² in the excited state. This extends a line of argument used to assign⁸⁴ the first reported vibrational quantum beats⁸⁵ and repeatedly since. The original line of argument is based on the Franck-Condon principle and even then depends on matching the femtosecond and resonance Raman wavelengths (for example, the dominant vibrational frequency in both femtosecond⁸¹ and resonance Raman⁸⁶ experiments switches from the fundamental to the second harmonic and back as the electronic excitation frequency is tuned across the absorption spectrum of I₂ in solution). Although the BChl a resonance Raman frequencies and FMO 2D oscillation frequencies are in oneto-one correspondence,² this is not a general characteristic of vibrational-excitonic resonance, which enhances vibrations around their excitonic resonance but may leave them below noise at other excitation frequencies.

D. The lowest exciton

The lowest exciton has a zero-point level for which the adiabatic approximation is reasonably accurate. Since the transition to this state carries almost all of the Franck-Condon absorption strength of the lowest exciton, the lowest exciton appears almost uncoupled in the absorption spectrum. Further, since relaxed emission proceeds from this state, for which an adiabatic description is valid, the relaxed emission spectrum obeys the Franck-Condon principle so far as relaxed emission from the uncoupled pigment does. However, in the presence of vibrational-excitonic resonance, higher vibrational levels of the lowest exciton are thoroughly mixed with higher exciton states so that higher vibrational levels and higher excitonic electronic states may not actually live long enough to be useful approximations for describing spectra at short times. 11,87

E. Circular dichroism spectra

Circular dichroism requires that the pigment transition dipoles be spatially arranged with some helicity. At the lowest level of theory, inclusion of vibrational-excitonic resonance need not dramatically change antenna circular dichroism spectra in comparison to modeling by the standard procedure⁸⁸ of dressing the circular dichroism stick spectrum from a disordered ensemble of purely electronic excitonic Hamiltonians with a narrowed line shape. Applying Kirkwood's coupled exciton theory of rotatory strength [Eq. (24) of Ref. 89 or Eq. (5a) of Ref. 90] to vibronic transitions from the zeropoint level to the upper states given by diagonalizing the vibronic interactions in Eq. (2) yields an unchanged rotatory strength for the lowest exciton transition, two transitions that sum to the rotatory strength of the upper exciton transition, plus Franck-Condon $\Delta v = 1$ transitions for each. Thus, the stick spectrum of optical rotatory linestrengths is different from that of a purely electronic model Hamiltonian, but the differences can be largely obscured by the anti-correlated gap ensemble average and correlated linewidths in the same manner as in the absorption spectrum. This suggests that the linewidth-broadened circular dichroism spectra are still useful for rough determination of the purely electronic coupling parameters of the excitonic states via standard analysis of the circular dichroism bands. A similar result was found by Won and Friesner for their more strongly coupled electron transfer Hamiltonian.⁶

F. Energy transfer mechanisms

At the quantum mechanical level, an energy transfer mechanism involves oscillatory transfer of energy back and forth between donor and acceptor that must be stopped so that energy becomes localized on the acceptor. Standard mechanisms for stopping these back and forth oscillations involve decoherence,³ which stops the oscillations and leads to an incoherent energy transfer rate, and vibrational energy relaxation,⁹¹ which makes the energy transfer irreversible by draining excess energy. For identical donor and acceptor pigments, we propose that conversion of their initially excited anticorrelated vibration into a correlated vibration is a potential mechanism for trapping electronic energy on the acceptor or at least delaying backward energy transfer. Trapping can occur through population transfer from the anti-correlated vibration to the correlated vibration (this population transfer is equivalent to decoherence between the two localized pigment vibrations). A temporary anti-correlated to correlated conversion can occur through vibrational inhomogeneity between donor and acceptor pigments, which may give rise to a back and forth anti-correlated to correlated quantum beat if the vibrational-excitonic resonance does not reassemble an anti-correlated mode. An effective vibrational inhomogeneity might arise from random thermal excitation of anharmonic vibrations on the separate pigments, thus causing a similar temporary conversion and delay of backwards energy transfer. One might think that such anharmonic processes could also play a role in hastening the anti-correlated beat decay on the ground electronic state of the antenna at higher temperatures; however, the bacteriochlorophyll a Raman linewidths appear to be dominated by coupling to discrete vibrations and are essentially independent of temperature, 51,92 suggesting that thermal variations in pigment vibrational frequencies arising from anharmonicity are not large enough to cause the reported temperature dependent beat decay.

G. Role of vibrational relaxation on the ground electronic state of the donor

As shown by the transformed matrix in Eq. (5) and the basis states in Eq. (6), basis states of $|\alpha\rangle$ and $|\beta\rangle$ excitonic character are coupled together by the vibrationally and electronically off-diagonal coupling $+(\mathbf{g}_d^{A-B}\sin(2\theta_d)\cdot\mathbf{\hat{q}})/2$. The resulting eigenstates obtained after numerically diagonalizing the exact Hamiltonian have a strongly mixed vibrational-electronic character from both the donor and acceptor pigments which allows non-adiabatic energy transfer from the donor to the acceptor. The nature of states on the acceptor pigment A that receive the electronic energy from the donor pigment B can be better understood by considering the second state in Eq. (6), with $|\alpha\rangle$ excitonic character and a quantum of excitation along the anti-correlated vibrational coordinate,

more carefully. The electronic character of this exciton is primarily composed of the electronically excited acceptor pigment A and the ground electronic state of the donor pigment B. The vibrational wavefunction has equal non-zero projections onto two localized vibrational states: one in which the acceptor pigment is vibrationally excited and one in which the donor pigment is left vibrationally excited. This means that the excess energy of the donor pigment can ultimately either be converted into a vibrational quantum on the excited electronic state of the acceptor (as assumed in the one-particle vibronic exciton or the coherent exciton scattering approximations^{9,10}) or be left behind as a vibrational quantum on the ground electronic state of the donor. This has an interesting consequence. The electronic energy transfer process is completed and made permanent by energetic relaxation down to the lowest vibrational state of the lowest exciton, the state written as $|A\rangle |G_B\rangle |v_A=0\rangle |v_B=0\rangle$ in the localized vibrational-site basis. Thus, vibrational relaxation on the electronically excited acceptor and the ground electronic state donor are equally important in completing energy transfer. It is important to point out that, from the excitonic point of view of the dimer as a whole, this latter relaxation path is still an electronic excited state relaxation process in that both states involved have an electronically excited acceptor and belong to the one-exciton manifold. Experimentally determining how this vibrational relaxation on the electronic ground state of the isolated pigment transforms into relaxation on the one-exciton manifold is essential for understanding how the ground electronic state vibrational relaxation processes of the uncoupled pigments contribute to stabilizing the final energy transfer product.

Some vibronic exciton models of photosynthetic energy transfer^{27,93} based on a Holstein-like Hamiltonian⁹⁴ explicitly exclude electronic energy transfer pathways that leave the ground state of the donor vibrationally excited (as discussed above). In such treatments, the coupling is restricted to proceed through the zero point level on the ground electronic state of the donor. Such a restriction also occurs based upon the Coherent Exciton Scattering (CES) approximation ¹⁰ (also called "one particle approximation"), which assumes that electronic excitation transfer from one monomer to the other is always accompanied by vibrational de-excitation of the donor. Davydov and Serikov's⁹¹ treatment of electronic energy transfer in the presence of a resonant vibration with exponential vibrational energy relaxation on the acceptor and exponential donor quenching also makes the same assumption that vibrational excitation strictly accompanies electronic excitation. With this assumption, the coupling between the exciton in one unit cell and the intramolecular vibrations in another unit cell is discarded, that is, "two-particle" states where at least one quantum of vibrational excitation resides in an electronically unexcited molecule are ignored. The analysis of Ref. 2 shows that this neglect reduces the energy transfer coupling matrix element by a factor of $\sqrt{2}$ (the ratio between the coupling to the anti-correlated vibration and the acceptor vibration). In the Golden rule rate equation limit, the factor of $\sqrt{2}$ in the coupling increases the energy transfer rate by a factor of 2 (see Paper I¹¹).

The "one particle" approximation might seem appropriate for strong exciton-phonon coupling such that the exciton

is accompanied by a vibrational distortion—in other words, for the excitonic energy transfer analog of a polaron in charge transfer. However, it cannot capture a finite vibrational distortion radius. Figure 1 and the supplementary material show that "one-particle" approximations throw away most of the coupling between states with multiple vibrational excitations. This incorrectly eliminates excitonic effects on vibrational progressions in the spectra (as in Ref. 14). Briggs and Herzenberg have discussed reasons why the coherent exciton scattering approximation and time dependent Hartree method fail for the electronic absorption spectra of dimers. 95

Considering the case of energy transfer between a donor and acceptor with the same energy gap $(E^A = E^B)$ provides additional insight into the role of vibrations with small Franck-Condon displacements in energy transfer. If a donor pigment is excited to v = 1 in the excited electronic state, it will have its strongest emission transition (with $\Delta v = 0$) to v = 1 in the ground electronic state. This emitted frequency overlaps with the strongest absorption transition of the acceptor, from v = 0 in the electronic ground state to v = 0 in the electronic excited state. This strongest actual emission/absorption path at a large distance becomes the strongest virtual emission/absorption path in Förster's resonant energy transfer at short distances. Note that leaving the vibration behind on the donor is the overwhelmingly dominant path (which is completely neglected by the "one particle approximation"). The "one particle" basis set has also been shown to be a bad approximation^{8,96} for organic semiconductors where significant nuclear rearrangements associated with charge or energy transport leave a "wake" of vibrational excitations behind.

It has been suggested that dissociation of vibronic excitons into separate vibrations and excitons is the characteristic feature of intermediate energy transfer coupling. Ontradicting this, the above discussion of the high vibronic exciton dissociation probability for very weak energy transfer coupling indicates vibronic exciton dissociation is not unique to intermediate energy transfer coupling. Vibronic excitons tend to hold together with strong coupling to vibrations and tend to dissociate with weak coupling to vibrations. This suggests that the more balanced dissociation probabilities discussed here might be a characteristic of energy transfer with intermediate coupling to vibrations.

V. CONCLUSIONS

This paper has treated non-adiabatic vibrational-electronic resonance on the excited state. Analysing the basis transformation from localized vibrational states $|v_A, v_B\rangle$ to delocalized vibrational states $|v_+, v_-\rangle$, it is shown that vibrational-electronic mixing near resonance allows for pathways where the electronic excitation from the donor is transferred to the acceptor so that the acceptor is both electronically and vibrationally excited, as well as pathways where an electronically de-excited donor is still vibrationally excited in its ground electronic state and the acceptor is electronically excited without excess vibrational energy. Both these pathways are treated on equal footing in the non-adiabatic energy transfer calculations here and in Ref. 2. Such

pathways where vibrational excitation is not strictly accompanied with an electronic excitation render the coherent exciton scattering approximation, made in a vibronic exciton model, invalid. A "one-particle" basis set neglects such pathways and therefore is unable to fully capture the excited state non-adiabatic dynamics and its consequences on the ground state of the antenna. Even under the adiabatic framework of Förster resonance energy transfer,³ the pathway that leaves the ground electronic state of the donor vibrationally excited can become dominant in the very weak vibrational displacement limit. In these circumstances, the concept of a polaron-like vibronic exciton does not appear to be useful. From a computational point of view, the use of one anti-correlated vibration seems preferable to the two particle basis because the single anti-correlated vibration can rigorously capture the full nonadiabatic dynamics.

Non-Condon effects are known to arise in individual chromophores based on porphyrins⁹⁸ and chlorophylls.^{36,82} In the dimer model presented here, it is assumed that the individual chromophores obey the Condon approximation. Some previous studies assumed the validity of the Condon approximation for both individual pigments and antennas. A crucial point here is that the Condon approximation still works for the correlated vibrations and for emission from the zero point level of the lowest exciton. However, in emission from the zero point on the lowest exciton, vibrational delocalization reduces the Huang-Rhys factors twofold (so that the two delocalized vibrations sum to the localized result in the absence of excitonic delocalization) and the Huang-Rhys factors for transitions to anti-correlated vibrations are further reduced by excitonic delocalization while the Huang-Rhys factors for the correlated vibrations are not affected further by excitonic delocalization. For the model considered here, such resonant vibrational-excitonic coupling effects appear to be more significant for vibrational satellite intensities than typical sitespecific changes in vibrational equilibrium or displacement. Higher excitonic eigenstates rapidly change electronic character as a function of anti-correlated nuclear coordinate so that the Condon approximation becomes invalid in the dimer even if it holds for individual pigments. For non-resonant vibrations, the anti-correlated vibrations have adiabatic changes in vibrational frequency that can exceed the typical site specific vibrational frequency shift. Thus, analysis of the spectra of pigment protein complexes should probably treat such vibronic effects on the anti-correlated vibrations and the non-additive nonadiabatic interactions between modes before considering site specific effects on vibrations. The combination of anti-correlated inhomogeneity and vibronic resonance qualitatively explains the absence of narrow satellite holes for higher excitons in photosynthetic antennas and the weakness of vibrational satellites, which arise only from correlated vibrations with displacements that are smaller than the isolated pigment. This reduces them below the typical noise level.

For the model considered here, the combined effects of intramolecular vibrations and environmental modes that couple to a single pigment are far from additive so that linear spectra appear to suppress the intensity of the environmental satellite. By including an additional near-resonant mode present in *BChl a*, we have shown that a finite width of non-adiabatic coupling around resonance relaxes the condition for exact resonance and might render such a non-adiabatic mechanism robust to changes in the protein environment. Within the resonance width, vibrational-excitonic resonance can reassemble a coupled vibrational state that has been split by weaker interactions. This reassembly is similar to the assembly of a more strongly coupled anti-correlated vibration from localized pigment vibrations. Nonadiabatic vibrational-excitonic resonance also offers design principles where structured environments can be engineered to exploit the width of non-adiabatic coupling operative in the presence of such modes.

SUPPLEMENTARY MATERIAL

See supplementary material for the localized to delocalized vibrational basis state transformation, information about numerical calculation of nonadiabatic eigenfunctions, the vibrational-excitonic coupling Hamiltonian matrix, the effects of the "one-particle" approximation in the displaced site basis, equations and line broadening models used to calculate absorption and emission spectra, and spectra from simulations with an environmental splitting of a vibration on either the donor or acceptor.

ACKNOWLEDGMENTS

We thank David Bocian (UC Riverside) for helpful discussions of bacteriochlorophyll Raman spectra. This material is based upon work supported by the National Science Foundation under Grant No. CHE-1405050 and by the Air Force Office of Scientific Research under AFOSR Award No. FA9550-14-1-0258. Any opinions, findings, and conclusions or recommendations expressed in this material are those of the authors and do not necessarily reflect the views of the National Science Foundation.

¹J. Franck and E. Teller, J. Chem. Phys. **6**, 861 (1938).

²V. Tiwari, W. K. Peters, and D. M. Jonas, Proc. Natl. Acad. Sci. U. S. A. 110, 1203 (2013).

³T. Förster, in *Modern Quantum Chemistry*, edited by O. Sinanoğlu (Academic Press, Inc., New York, 1965), p. 93.

⁴R. Friesner and R. Wertheimer, Proc. Natl. Acad. Sci. U. S. A. **79**, 2138 (1982); **79**, 5752 (1982).

⁵Y. Won and R. A. Friesner, Proc. Natl. Acad. Sci. U. S. A. 84, 5511 (1987);
 J. Phys. Chem. 92, 2214 (1988).

⁶Y. Won and R. A. Friesner, J. Phys. Chem. **92**, 2208 (1988).

⁷E. J. P. Lathrop and R. A. Friesner, J. Phys. Chem. **98**, 3050 (1994); **98**, 3056 (1994).

⁸F. C. Spano, Acc. Chem. Res. **43**, 429 (2009).

⁹M. R. Philpott, J. Chem. Phys. **47**, 4437 (1967).

¹⁰J. Roden, A. Eisfeld, and J. S. Briggs, Chem. Phys. **352**, 258 (2008).

¹¹V. Tiwari, W. K. Peters, and D. M. Jonas, J. Chem. Phys. **147**, 154308 (2017).

¹²M. Schröter, S. D. Ivanov, J. Schulze, S. P. Polyutov, Y. Yan, T. Pullerits, and O. Kühn, Phys. Rep. **567**, 1 (2015).

¹³O. Kühn and V. May, Charge and Energy Transfer Dynamics in Molecular Systems, 2nd Revised and Enlarged ed. (Wiley-VCH, 2004).

¹⁴C. Friedl, T. Renger, H. v. Berlepsch, K. Ludwig, M. Schmidt am Busch, and J. Megow, J. Phys. Chem. C 120, 19416 (2016).

¹⁵T. Pullerits, D. Zigmantas, and V. Sundström, Proc. Natl. Acad. Sci. U. S. A. **110**, 1148 (2013).

¹⁶M. T. W. Milder, B. Brüggemann, R. van Grondelle, and J. L. Herek, Photosynth. Res. **104**, 257 (2010).

- ¹⁷P. W. Foster, W. K. Peters, and D. M. Jonas, Chem. Phys. Lett. **683**, 268 (2017).
- ¹⁸J. S. Briggs and A. Herzenberg, J. Phys. B: At. Mol. Phys. 3, 1663 (1970); Mol. Phys. 21, 865 (1971).
- ¹⁹M. R. Philpott, J. Chem. Phys. **47**, 2534 (1967).
- ²⁰W. Siebrand, J. Chem. Phys. **40**, 2223 (1964).
- ²¹M. Dahlbom, W. Beenken, V. Sundström, and T. Pullerits, Chem. Phys. Lett. 364, 556 (2002).
- ²²F. C. Spano, Chem. Phys. **325**, 22 (2006).
- ²³ D. A. Farrow, E. R. Smith, W. Qian, and D. M. Jonas, J. Chem. Phys. 129, 174509 (2008).
- ²⁴K. Huang and A. Rhys, Proc. R. Soc. A **204**, 406 (1950); S. Mukamel, Principles of Nonlinear Spectroscopy (Oxford University Press, New York, 1995), Vol. 6.
- ²⁵J. Schulze, M. Torbjörnsson, O. Kühn, and T. Pullerits, New J. Phys. 16, 045010 (2014).
- ²⁶F. C. Spano and H. Yamagata, J. Phys. Chem. B **115**, 5133 (2011).
- ²⁷J. M. Womick and A. M. Moran, J. Phys. Chem. B **115**, 1347 (2011).
- ²⁸M. Rätsep and A. Freiberg, J. Lumin. **127**, 251 (2007).
- ²⁹N. Herascu, A. Kell, K. Acharya, R. Jankowiak, R. E. Blankenship, and V. Zazubovich, J. Phys. Chem. B 118, 2032 (2014).
- ³⁰H. P. Lamichhane and G. Hastings, Proc. Natl. Acad. Sci. U. S. A. 108, 10526 (2011).
- ³¹J. M. Hughes, M. C. Hutter, J. R. Reimers, and N. S. Hush, J. Am. Chem. Soc. **123**, 8550 (2001).
- ³²C. Rischel, D. Spiedel, J. P. Ridge, M. R. Jones, J. Breton, J.-C. Lambry, J.-L. Martin, and M. H. Vos, Proc. Natl. Acad. Sci. U. S. A. 95, 12306 (1998).
- ³³S. I. E. Vulto, M. A. de Baat, R. J. W. Louwe, H. P. Permentier, T. Neef, M. Miller, H. van Amerongen, and T. J. Aartsma, J. Phys. Chem. B 102, 9577 (1998); M. Rätsep and A. Freiberg, Chem. Phys. Lett. 434, 306 (2007).
- ³⁴M. Wendling, T. Pullerits, M. A. Przyjalgowski, S. I. E. Vulto, T. J. Aartsma, R. van Grondelle, and H. van Amerongen, J. Phys. Chem. B **104**, 5825 (2000).
- ³⁵J. R. Diers and D. F. Bocian, J. Am. Chem. Soc. **117**, 6629 (1995).
- ³⁶M. Rätsep, Z.-L. Cai, J. R. Reimers, and A. Freiberg, J. Chem. Phys. 134, 024506 (2011).
- ³⁷V. Zazubovich, I. Tibe, and G. J. Small, J. Phys. Chem. B **105**, 12410 (2001).
- ³⁸M. Cho, H. M. Vaswani, T. Brixner, J. Stenger, and G. R. Fleming, J. Phys. Chem. B **109**, 10542 (2005).
- ³⁹ J. Adolphs and T. Renger, Biophys. J. **91**, 2778 (2006).
- ⁴⁰T. Renger, A. Klinger, F. Steinecker, M. Schmidt am Busch, J. Numata, and F. Müh, J. Phys. Chem. B 116, 14565 (2012).
- ⁴¹S. Savikhin, D. R. Buck, and W. S. Struve, Chem. Phys. **223**, 303 (1997).
- ⁴² A. Kell, K. Acharya, R. E. Blankenship, and R. Jankowiak, Photosynth. Res. 120, 323 (2014).
- ⁴³ A. Kell, K. Acharya, V. Zazubovich, and R. Jankowiak, J. Phys. Chem. Lett. 5, 1450 (2014).
- ⁴⁴S. Mukamel, *Principles of Nonlinear Optical Spectroscopy* (Oxford University Press, New York, 1995), Vol. 6.
- ⁴⁵ Y. Tanimura and S. Mukamel, Phys. Rev. E 47, 118 (1993); Y. Gu, A. Widom, and P. M. Champion, J. Chem. Phys. 100, 2547 (1994).
- ⁴⁶S. M. Gallagher Faeder and D. M. Jonas, Phys. Rev. A **62**, 033820 (2000).
- ⁴⁷D. A. Farrow, W. Qian, E. R. Smith, A. A. Ferro, and D. M. Jonas, J. Chem. Phys. **128**, 144510 (2008); K. A. Kitney-Hayes, A. W. Albrecht-Ferro, V. Tiwari, and D. M. Jonas, *ibid.* **140**, 124312 (2014).
- ⁴⁸E. U. Condon, Am. J. Phys. **15**, 365 (1947).
- 49 From the adiabatic perspective used in Ref. 2, the unequal line strengths at diabatic vibrational-excitonic resonance reflect both intensity interference effects arising from the Franck-Condon intensity for $\Delta v = 1$ transitions and a difference between vibrational frequencies for the adiabatic potential curves of the two excitons, which shifts the resonance.
- ⁵⁰ V. Tiwari, P. W. Foster, and D. M. Jonas, "Electronic energy transfer through non-adiabatic vibrational-electronic resonance. III. 2D spectra for a dimer," J. Chem. Phys. (unpublished).
- ⁵¹K. Czarnecki, J. R. Diers, V. Chynwat, J. P. Erickson, H. A. Frank, and D. F. Bocian, J. Am. Chem. Soc. 119, 415 (1997).
- ⁵²D. J. Nesbitt and R. W. Field, J. Phys. Chem. **100**, 12735 (1996).
- ⁵³ A. Roitberg, R. Gerber, R. Elber, and M. Ratner, Science **268**, 1319 (1995).
- ⁵⁴M. A. Steffen, K. Lao, and S. G. Boxer, Science **264**, 810 (1994).
- ⁵⁵T. F. Soules and C. B. Duke, Phys. Rev. B **3**, 262 (1971).
- ⁵⁶E. L. Read, G. S. Schlau-Cohen, G. S. Engel, J. Wen, R. E. Blankenship, and G. R. Fleming, Biophys. J. 95, 847 (2008).

- ⁵⁷K. K. Rebane, in *Zero Phonon Lines and Spectral Hole Burning in Spectroscopy and Photochemistry*, edited by O. Sild and K. Haller (Springer-Verlag, Berlin, 1988); K. K. Rebane, *Impurity Spectra of Solids* (Plenum Press, New York, 1970).
- ⁵⁸Y. Fujihashi, G. R. Fleming, and A. Ishizaki, J. Chem. Phys. **142**, 212403 (2015).
- ⁵⁹M. H. Lee and A. Troisi, J. Chem. Phys. **146**, 075101 (2017).
- ⁶⁰Z. Zhao and F. C. Spano, J. Phys. Chem. C **111**, 6113 (2007).
- ⁶¹M. Higashi and S. Saito, J. Chem. Theory Comput. **12**, 4128 (2016); M. K. Lee and D. F. Coker, J. Phys. Chem. Lett. **7**, 3171 (2016).
- ⁶²R. K. Clayton, *Photosynthesis: Physical Mechanisms and Chemical Patterns* (Cambridge University Press, Cambridge, 1980).
- ⁶³R. E. Blankenship, Molecular Mechanisms of Photosynthesis (Blackwell Science Ltd., 2002).
- ⁶⁴J. G. Radziszewski, J. Waluk, M. Nepras, and J. Michl, J. Phys. Chem. **95**, 1963 (1991); K. V. Berezin and V. V. Nechaev, J. Appl. Spectrosc. **69**, 801 (2002).
- ⁶⁵J. R. Diers, Q. Tang, C. J. Hondros, C.-Y. Chen, D. Holten, J. S. Lindsey, and D. F. Bocian, J. Phys. Chem. B 118, 7520 (2014).
- ⁶⁶R. A. Marcus, Angew. Chem., Int. Ed. Engl. **32**, 1111 (1993).
- ⁶⁷J. Jortner, Biochim. Biophys. Acta, Rev. Bioenerg. **594**, 193 (1980).
- ⁶⁸P. J. O'Malley, J. Am. Chem. Soc. **122**, 7798 (2000).
- ⁶⁹A. Warshel, Proc. Natl. Acad. Sci. U. S. A. 77, 3105 (1980).
- ⁷⁰K. L. Dillman and W. F. Beck, J. Phys. Chem. B **114**, 15269 (2010).
- J. R. Diers and D. F. Bocian, J. Phys. Chem. 98, 12884 (1994).
 F. D. Fuller, J. Pan, A. Gelzinis, V. Butkus, S. S. Senlik, D. E. Wilcox, C. F. Yocum, L. Valkunas, D. Abramavicius, and J. P. Ogilvie, Nat. Chem.
- 6, 706 (2014).
 ⁷³E. Romero, R. Augulis, V. I. Novoderezhkin, M. Ferretti, J. Thieme, D. Zigmantas, and R. van Grondelle, Nat. Phys. 10, 676 (2014).
- ⁷⁴R. Jankowiak, M. Reppert, V. Zazubovich, J. Pieper, and T. Reinot, Chem. Rev. 111, 4546 (2011).
- ⁷⁵S. G. Johnson and G. J. Small, J. Phys. Chem. **95**, 471 (1991).
- ⁷⁶E. M. Franken, S. Neerken, R. J. W. Louwe, J. Amesz, and T. J. Aartsma, Biochemistry 37, 5046 (1998).
- ⁷⁷R. J. W. Louwe, J. Vrieze, A. J. Hoff, and T. J. Aartsma, J. Phys. Chem. B 101, 11280 (1997).
- Adolphs, M. Berrer, and T. Renger, J. Am. Chem. Soc. 138, 2993 (2016).
 J. Yuen-Zhou, J. J. Krich, and A. Aspuru-Guzik, J. Chem. Phys. 136, 234501 (2012).
- ⁸⁰W. T. Pollard and R. A. Mathies, Annu. Rev. Phys. Chem. 43, 497 (1992); D. M. Jonas and G. R. Fleming, in *Ultrafast Processes in Chemistry and Photobiology*, edited by M. A. El-Sayed, I. Tanaka, and Y. Molin (Blackwell Scientific, Oxford, 1995), p. 225.
- ⁸¹D. M. Jonas, S. E. Bradforth, S. A. Passino, and G. R. Fleming, J. Phys. Chem. **99**, 2594 (1995).
- ⁸²M. Umetsu, Z.-Y. Wang, K. Yoza, M. Kobayashi, and T. Nozawa, Biochim. Biophys. Acta 1457, 106 (2000); J. R. Reimers, Z.-L. Cai, R. Kobayashi, M. Rätsep, A. Freiberg, and E. Krausz, Sci. Rep. 3, 2761 (2013).
- ⁸³D. Hayes, G. B. Griffin, and G. S. Engel, Science **340**, 1431 (2013).
- ⁸⁴K. A. Nelson and L. Williams, Phys. Rev. Lett. **58**, 745 (1987).
- 85 M. J. Rosker, F. W. Wise, and C. L. Tang, Phys. Rev. Lett. 57, 321 (1986).
- ⁸⁶R. J. Sension and H. L. Strauss, J. Chem. Phys. 85, 3791 (1986).
- ⁸⁷W. K. Peters, V. Tiwari, and D. M. Jonas, J. Chem. Phys. **147**, 194306 (2017).
- ⁸⁸O. J. G. Somsen, R. van Grondelle, and H. van Amerongen, Biophys. J. 71, 1934 (1996); H. Van Amerongen, L. Valkunas, and R. Van Grondelle, *Photosynthetic Excitons* (World Scientific, Singapore, 2000).
- ⁸⁹J. G. Kirkwood, J. Chem. Phys. **5**, 479 (1937).
- ⁹⁰E. U. Condon, Rev. Mod. Phys. **9**, 432 (1937).
- 91 A. S. Davydov and A. A. Serikov, Phys. Status Solidi B 51, 57 (1972).
- ⁹² V. Palaniappian, M. A. Aldema, H. A. Frank, and D. F. Bocian, Biochemistry 31, 11050 (1992).
- ⁹³N. Christensson, H. F. Kauffmann, T. Pullerits, and T. Mančal, J. Phys. Chem. B 116, 7449 (2012); A. Chenu, N. Christensson, H. F. Kauffmann, and T. Mančal, Sci. Rep. 3, 2029 (2013).
- ⁹⁴T. Holstein, Ann. Phys. **8**, 325 (1959).
- ⁹⁵J. S. Briggs and A. Herzenberg, Mol. Phys. **23**, 203 (1972).
- ⁹⁶M. Andrzejak and P. Petelenz, Chem. Phys. **335**, 155 (2007).
- ⁹⁷A. Witkowski, in *Modern Quantum Chemistry, Part III: Action of Light and Organic Crystals*, edited by O. Sinanoğlu (Academic Press, New York, 1965).
- ⁹⁸T. G. Spiro and T. C. Strekas, Proc. Natl. Acad. Sci. U. S. A. **69**, 2622 (1972).

SUPPLEMENTARY MATERIAL

for

Electronic Energy Transfer through Non-Adiabatic Vibrational-Electronic Resonance. II: 1D Spectra for a Dimer

Vivek Tiwari and David M. Jonas

Department of Chemistry and Biochemistry

University of Colorado, Boulder, CO 80309-0215

S1. Localized To Delocalized Vibrational State Transformation

This transformation is illustrated explicitly for harmonic oscillator eigenfunctions with a total of two quanta of vibrational excitation. The undisplaced vibrational basis functions of the ground electronic state are used for all electronic states in each coordinate system. In dimensionless normal coordinates, the square normalized harmonic oscillator eigenfunctions are:

$$\langle q | v = 0 \rangle = \pi^{-1/4} \exp(-q^2/2);$$
 (SM1)a

$$\langle q | v = 1 \rangle = 2^{1/2} q \pi^{-1/4} \exp(-q^2 / 2) = 2^{1/2} q \langle q | v = 0 \rangle;$$
 (SM1)b

$$\langle q | v = 2 \rangle = 2^{-1/2} (2q^2 - 1) \pi^{-1/4} \exp(-q^2 / 2) = 2^{-1/2} (2q^2 - 1) \langle q | v = 0 \rangle.$$
 (SM1)c

Defining a shorthand notation with the first equality on each line below, the localized two quanta basis states have the coordinate representations

$$(2_A, 0_B) = \langle q_A | v_A = 2 \rangle \langle q_B | v_B = 0 \rangle = 2^{-1/2} (2q_A^2 - 1) \psi_{00}$$
 (SM2)a

$$(0_A, 2_B) = \langle q_A | v_A = 0 \rangle \langle q_B | v_B = 2 \rangle = 2^{-1/2} (2q_B^2 - 1) \psi_{00}$$
 (SM2)b

$$(1_A, 1_B) = \langle q_A | v_A = 1 \rangle \langle q_B | v_B = 1 \rangle = 2q_A q_B \psi_{00}.$$
 (SM2)c

The last equality on each line factors out the 2D Gaussian zero point eigenfunction $\psi_{00} = \langle q_A | v_A = 0 \rangle \langle q_B | v_B = 0 \rangle = \langle q_+ | v_+ = 0 \rangle \langle q_- | v_- = 0 \rangle$, which is common to all harmonic oscillator eigenfunctions, in order to emphasize the relationships between eigenfunctions. Similarly, the delocalized two quanta basis states have the coordinate representations

$$(2_+, 0_-) = \langle q_+ | v_+ = 2 \rangle \langle q_- | v_- = 0 \rangle = 2^{-1/2} (2q_+^2 - 1) \psi_{00}$$
 (SM3)a

$$(0_+, 2_-) = \langle q_+ | v_+ = 0 \rangle \langle q_- | v_- = 2 \rangle = 2^{-1/2} (2q_-^2 - 1) \psi_{00}$$
 (SM3)b

$$(1_+, 1_-) = \langle q_+ | v_+ = 1 \rangle \langle q_- | v_- = 1 \rangle = 2q_+ q_- \psi_{00}.$$
 (SM3)c

So, expressing the delocalized coordinates in terms of the localized coordinates by substituting

$$q_{+} = (q_{A} + q_{B})2^{-1/2}$$
 (SM4)a

and
$$q_{-} = (q_A - q_B)2^{-1/2}$$
 (SM4)b

into Eq. (SM3) gives

$$(2_+, 0_-) = 2^{-1/2} (q_A^2 + 2q_A q_B + q_B^2 - 1) \psi_{00}$$
(SM5)a

$$(0_+, 2_-) = 2^{-1/2} (q_A^2 - 2q_A q_B + q_B^2 - 1) \psi_{00}.$$
 (SM5)b

and
$$(1_+, 1_-) = (q_A^2 - q_B^2)\psi_{00}$$
. (SM5)c

Writing the delocalized states in Eq. (SM5) as linear combinations of the localized states in Eq. (SM2), we obtain the equalities

$$(2_+, 0_-) = (1/2)[(2_A, 0_B) + (0_A, 2_B)] + 2^{-1/2}(1_A, 1_B),$$
 (SM6)a

$$(0_+, 2_-) = (1/2)[(2_A, 0_B) + (0_A, 2_B)] - 2^{-1/2}(1_A, 1_B),$$
 (SM6)b

and
$$(1_+, 1_-) = 2^{-1/2}[(2_A, 0_B) - (0_A, 2_B)].$$
 (SM6)c

that give the basis state transformation. Eq. (SM6) shows that the vibrational basis state $(2_+, 0_-)$ with two quanta of correlated vibration involves all three isoenergetic localized vibrational basis

states. The same holds for two quanta of anti-correlated vibration $(0_+, 2_-)$. In the localized vibrational basis, all three of these basis states have systematic interference effects in their vibrational-excitonic coupling. In contrast, linear vibrational-excitonic coupling is much simpler in the delocalized basis, which has $\Delta v_+ = 0$ and $\Delta v_- = \pm 1$ selection rules so long as the undisplaced vibrational basis functions of the ground electronic state are used. If the vibrational basis functions are displaced to the equilibrium geometry of each electronic state, the $\Delta v_+ = 0$ selection rule is loosened by Franck-Condon overlap integrals, with a similar modification of the $\Delta v_- = \pm 1$ rule for linear vibrational-excitonic coupling.

S2. Exact Hamiltonian Diagonalization

All calculations described in the text were carried out in a complete site basis for two pigments A and B, with three dimer electronic states $|0_A\rangle|0_B\rangle$, $|A\rangle|0_B\rangle$, $|0_A\rangle|B\rangle$. In the dimer electronic state $|A\rangle|0_B\rangle$, pigment A is electronically excited while pigment B is in the ground electronic state, and so on. Each pigment has either one or two vibrational modes, so that the dimer has up to 4 vibrational modes. These modes are represented in a site basis, which means that a given coordinate i has its equilibrium displaced [nonzero d_i^A or d_i^B in Eq. (1)] upon electronic excitation of either pigment A or pigment B, but not both. For each dimer electronic state, the dimer vibronic basis states are obtained by a direct product of the dimer vibrational basis with the dimer electronic basis. For instance, with one intramolecular vibrational mode on each pigment, the dimer vibronic basis states associated with the dimer electronic state $|A\rangle|0_B\rangle$, include $|A\rangle|0_B\rangle|v_A\rangle|v_B\rangle$ for all non-negative values of v_A and v_B . For simplicity in evaluating coupling and transition dipole matric elements, the undisplaced vibrational basis of the ground

electronic state is used for calculations. Harmonic oscillator matrix elements of the coordinate operators in the Hamiltonian are taken from Papousek and Aliev. In practice, this basis must be truncated above some quantum number for numerical diagonalization. For the case of one intramolecular vibrational mode on each pigment, or one intramolecular vibrational mode on each pigment and an environmental mode, 9 vibrational basis states for each mode (v=0 to v=8) were included in the numerical Hamiltonian on each pigment electronic state. This gives a total of 81 vibrational basis states on the ground electronic state of the dimer and a total of 162 vibronic basis states on the excited electronic state of the dimer. For the case of two intramolecular vibrational modes on each pigment, 7 vibrational basis states for each mode were included on each pigment electronic state (4802 vibronic basis states). These basis sets satisfactorily converge the low energy states accessed in the spectra at temperatures up to 80K.

Matrix elements for the Hamiltonian in Eq. 1 of the text are shown below for the case of one intramolecular vibrational mode per pigment with vibrational frequency ω for both pigments. The matrix below only shows 2 vibrational basis states for each mode on each excited electronic state of the dimer. The rows and columns of the matrix are labeled $A_{v_Av_B}$ or $B_{v_Av_B}$, depending on which pigment is excited, with right subscripts on A or B denoting the vibrational quantum numbers v_A and v_B . Notice that the direct product basis used below allows non-zero v_B on the dimer electronic state A for which pigment B is in its ground electronic state.

	A_{00}	A_{10}	A_{01}	A_{11}	B_{00}	B_{10}	B_{01}	B_{11}
A_{00}	$E_{\scriptscriptstyle A}$	$-\omega d/\sqrt{2}$	0	0	J	0	0	0
A_{10}	$-\omega d/\sqrt{2}$	$E_A + \omega$	0	0	0	J	0	0
A_{01}	0	0	$E_{\scriptscriptstyle A}+\omega$	$-\omega d/\sqrt{2}$	0	0	J	0
A_{11}	0	0	$-\omega d/\sqrt{2}$	$E_A + 2\omega$	0	0	0	J
B_{00}	J	0	0	0	$E_{\scriptscriptstyle B}$	0	$-\omega d/\sqrt{2}$	0
B_{10}	0	J	0	0	0	$E_B + \omega$	0	$-\omega d/\sqrt{2}$
B_{01}	0	0	J	0	$-\omega d/\sqrt{2}$	0	$E_B + \omega$	0
B_{11}	0	0	0	J	0	$-\omega d/\sqrt{2}$	0	$E_B + 2\omega$

S3. Comparison to One-Particle Approximations

In contrast to the above exact Hamiltonian, the corresponding Hamiltonian CES approximation or one particle vibronic exciton model is shown below. These one particle approximations eliminate all states in which electronic and vibrational excitation reside on different molecules (for example, v_B is restricted to zero in electronic state A). States such as A_{01} and B_{10} , and A_{11} and B_{11} are not allowed by the one-particle approximation and are simply eliminated. Since, in the exact Hamiltonian, pairs such as A_{01} and B_{01} have a direct Coulombic coupling J, simple elimination of states such as A_{01} effectively eliminates all *direct* Coulombic coupling between vibrationally excited states of the dimer. This direct Coulombic coupling occurs through dimer excited electronic states with vibrational excitation on the ground electronic state of one pigment. For example, coupling between A_{01} and B_{01} is eliminated because the dimer excited electronic state A_{01} has pigment B in its ground electronic state but with a quantum of vibrational excitation, which disallows it in the one-particle basis. This leaves only A_{00} and B_{00} with direct Coulombic coupling in the one particle approximation.

If one transforms the above matrix (extended to include all states A_{n0} and B_{0n}) so as to diagonalize the Franck-Condon displacement, one obtains

$$A_{00} \qquad A_{10} \qquad B_{00} \qquad B_{01}$$

$$A_{00} \qquad E_{A} - \lambda \qquad 0 \qquad J \langle 0^{A} | 0^{G} \rangle \langle 0^{G} | 0^{B} \rangle \qquad J \langle 0^{A} | 0^{G} \rangle \langle 0^{G} | 1^{B} \rangle$$

$$A_{10} \qquad 0 \qquad E_{A} - \lambda + \omega \qquad J \langle 1^{A} | 0^{G} \rangle \langle 0^{G} | 0^{B} \rangle \qquad J \langle 1^{A} | 0^{G} \rangle \langle 0^{G} | 1^{B} \rangle$$

$$B_{00} \qquad J \langle 0^{B} | 0^{G} \rangle \langle 0^{G} | 0^{A} \rangle \qquad J \langle 0^{B} | 0^{G} \rangle \langle 0^{G} | 1^{A} \rangle \qquad E_{B} - \lambda \qquad 0$$

$$B_{01} \qquad J \langle 1^{B} | 0^{G} \rangle \langle 0^{G} | 0^{A} \rangle \qquad J \langle 1^{B} | 0^{G} \rangle \langle 0^{G} | 1^{A} \rangle \qquad 0 \qquad E_{B} - \lambda + \omega$$

As can be seen, in the one particle approximation, all couplings except $A_{00} - B_{00}$ become indirect in the sense that they are borrowed or stolen from the one retained direct Coulombic coupling by Franck-Condon overlap integrals. The couplings are color coded according to the leading power of the displacement in the Franck-Condon overlap integrals (blue for 0^{th} , green for 1^{st} , pink for 2^{nd}). When the vibrational displacement is small, the largest coupling between vibrationally excited states in the one-particle basis is attenuated by a small Franck-Condon factor.

Matrix up to v=1 states for the complete Hamiltonian in the harmonic vibrational basis that is displaced to the equilibrium of each electronic state:

	A_{00}	A_{10}	A_{01}	A_{11}	B_{00}	B_{10}	B_{01}	B_{11}
A_{00}	$E_{_A}\!-\!\lambda$	0	0	0	$Jig\langle 0^{A}ig 0^{G}ig angleig\langle 0^{G}ig 0^{B}ig angle$	$J \left< 0^4 \left 1^G \right> \left< 0^G \left 0^B \right> \right.$	$J \left< 0^4 \left 0^G \right> \left< 0^G \left 1^B \right> \right.$	$J\left\langle 0^{A}\left 1^{G}\right\rangle \left\langle 0^{G}\left 1^{B}\right\rangle \right.$
A_{10}	0	$E_{_{A}}-\lambda+\omega$	0	0	$Jig\langle 1^{A}ig 0^{G}ig angleig\langle 0^{G}ig 0^{B}ig angle$	$Jig\langle 1^{A}ig 1^{G}ig angleig\langle 0^{G}ig 0^{B}ig angle$	$J \left\langle 1^{4} \left 0^{G} \right\rangle \left\langle 0^{G} \left 1^{B} \right\rangle \right.$	$J \left< 1^A \left 1^G \right> \left< 0^G \left 1^B \right> \right.$
A_{01}	0	0	$E_{_A} - \lambda + \omega$	0	$J\left\langle 0^{4}\left 0^{G} ight angle \left\langle 1^{G}\left 0^{B} ight angle$	$Jig\langle 0^{A}ig 1^{G}ig angleig\langle 1^{G}ig 0^{B}ig angle$	$Jig\langle 0^4 \left 0^G ight angle ig\langle 1^G \left 1^B ight angle$	$J\left\langle 0^{A}\left 1^{G}\right\rangle \left\langle 1^{G}\left 1^{B}\right\rangle \right.$
A_{11}	0	0	0	$E_{_A} - \lambda + 2\omega$	$J\left\langle 1^{A}\left 0^{G} ight angle \left\langle 1^{G}\left 0^{B} ight angle$	$Jig\langle 1^{A}ig 1^{G}ig angleig\langle 1^{G}ig 0^{B}ig angle$	$Jig\langle 1^{A}ig 0^{G}ig angleig\langle 1^{G}ig 1^{B}ig angle$	$Jig\langle 1^{A}ig 1^{G}ig angleig\langle 1^{G}ig 1^{B}ig angle$
B_{00}	$Jig\langle 0^B ig 0^G ig angle ig\langle 0^G ig 0^4 ig angle$	$Jig\langle 0^Big 0^Gig angleig\langle 0^Gig 1^4ig angle$	$Jig\langle 0^B \left 1^G ig angle ig\langle 0^G \left 0^A ight angle$	$J\left\langle 0^{B}\left 1^{G} ight angle \left\langle 0^{G}\left 1^{A} ight angle$	$E_{\scriptscriptstyle B} - \lambda$	0	0	0
B_{10}	$J\left\langle 0^{B}\left 0^{G} ight angle \left\langle 1^{G}\left 0^{A} ight angle$		$J\left\langle 0^{B}\left 1^{G} ight angle \left\langle 1^{G}\left 0^{A} ight angle$	$Jig\langle 0^Big 1^Gigigig\langle 1^Gig 1^Aigig angle$	0	$E_{_B} - \lambda + \omega$	0	0
B_{01}	$J \left< 1^B \left 0^G \right> \left< 0^G \left 0^A \right> \right.$	$Jig\langle 1^B ig 0^G ig angle ig\langle 0^G ig 1^A ig angle$	$Jig\langle 1^{B}ig 1^{G}ig angleig\langle 0^{G}ig 0^{A}ig angle$	$J \left\langle 1^{B} \left 1^{G} \right\rangle \left\langle 0^{G} \left 1^{A} \right\rangle \right.$	0	0	$E_{\scriptscriptstyle B} - \lambda + \omega$	0
B_{11}	$J \left\langle 1^B \left 0^G \right\rangle \left\langle 1^G \left 0^4 \right\rangle \right.$	$J \Big\langle 1^B \big 0^G \Big\rangle \Big\langle 1^G \big 1^4 \Big\rangle$	$J\left\langle 1^{B}\left 1^{G} ight angle \left\langle 1^{G}\left 0^{A} ight angle$	$J \left\langle 1^{B} \left 1^{G} ight angle \left\langle 1^{G} \left 1^{4} ight angle$	0	0	0	$E_{\scriptscriptstyle B} - \lambda + 2\omega$

Matrix up to v=1 states for the one-particle approximate Hamiltonian in the harmonic vibrational basis that is displaced to the equilibrium of each electronic state:

$$A_{00} = A_{10} = A_{10} = B_{00} = B_{01}$$

$$A_{00} = E_{A} - \lambda = 0 = J \langle 0^{A} | 0^{G} \rangle \langle 0^{G} | 0^{B} \rangle = J \langle 0^{A} | 0^{G} \rangle \langle 0^{G} | 1^{B} \rangle$$

$$A_{10} = 0 = E_{A} - \lambda + \omega = J \langle 1^{A} | 0^{G} \rangle \langle 0^{G} | 0^{B} \rangle = J \langle 1^{A} | 0^{G} \rangle \langle 0^{G} | 1^{B} \rangle$$

$$B_{00} = J \langle 0^{B} | 0^{G} \rangle \langle 0^{G} | 0^{A} \rangle = J \langle 1^{B} | 0^{G} \rangle \langle 0^{G} | 1^{A} \rangle = E_{B} - \lambda = 0$$

$$B_{01} = J \langle 1^{B} | 0^{G} \rangle \langle 0^{G} | 0^{A} \rangle = J \langle 1^{B} | 0^{G} \rangle \langle 0^{G} | 1^{A} \rangle = 0$$

$$E_{B} - \lambda + \omega$$

S4. Calculation of Absorption and Emission Cross-Sections

For the calculations presented here, the exact dimer Hamiltonian in Eq. (1) of the main text is numerically diagonalized, resulting in numerically exact non-adiabatic eigenvectors. For the case of one intramolecular vibrational mode per pigment, the n^{th} eigenvector is given by

$$\left|\psi_{n}\right\rangle = \sum_{v_{A}, v_{B}} c_{nv_{A}v_{B}}^{A} \left|A\right\rangle \left|0_{B}\right\rangle \left|v_{A}\right\rangle \left|v_{B}\right\rangle + c_{nv_{A}v_{B}}^{B} \left|0_{A}\right\rangle \left|B\right\rangle \left|v_{A}\right\rangle \left|v_{B}\right\rangle. \tag{SM7}$$

Since the undisplaced vibrational basis of the ground electronic state is used for all electronic states, the transition dipole vector between vibrational state (v_A, v_B) on the ground electronic state of the dimer $|0_A\rangle|0_B\rangle|v_A\rangle|v_B\rangle$ and nonadiabatic eigenstate $|\psi_n\rangle$ on the excited electronic state of the dimer is given by

$$\mu_{0v_{A}v_{R},n} = c_{nv_{A}v_{R}}^{A} \mu_{0,A} + c_{nv_{A}v_{R}}^{B} \mu_{0,B}$$
(SM8)

where $\mu_{0,A} = \langle 0 | \hat{\mu} | A \rangle = \mu_A \hat{e}_A$ and $\mu_{0,B} = \langle 0 | \hat{\mu} | B \rangle = \mu_B \hat{e}_B$. The transition dipoles are assumed to be perpendicular and equal in magnitude, that is, $\hat{e}_A \perp \hat{e}_B$ and $\mu_A = \mu_B$.

Once the transition dipoles are calculated, the stick absorption and stimulated emission cross sections are given by² –

$$\sigma_{abs}(\omega) \simeq \sum_{n,0,\nu_{A},\nu_{B}} \omega p_{0\nu_{A}\nu_{B}} |\mu_{n0\nu_{A}\nu_{B}}|^{2} \delta(\omega - \omega_{n0\nu_{A}\nu_{B}})$$

$$\sigma_{em}(\omega) \simeq \sum_{n,0,\nu_{A},\nu_{B}} \omega p_{n} |\mu_{0\nu_{A}\nu_{B}n}|^{2} \delta(\omega - \omega_{0\nu_{A}\nu_{B}n})$$
(SM9)

The similarity symbol is used only because constants of proportionality have been omitted. For absorption starting from ground electronic state of the dimer, the Boltzmann factor $p_{0\nu_A\nu_B}$ gives the temperature dependent occupation probability of the state with v_A and v_B quanta of vibrational excitation on pigments A and B, respectively. For emission starting from the relaxed

excited electronic state of the dimer, the Boltzmann factor p_n gives the temperature dependent occupation probability of the n^{th} nonadiabatic eigenstate.

Electronic decoherence between zero and one-quantum electronic states is caused by correlated and anti-correlated phonons, and leads to broadening of the absorption and emission stick spectra. The correlated part of the broadening can be rigorously included in the calculation by convolution with the nonadiabatic spectra.³ Here, all of the line broadening is approximately included by modeling the low-energy phonon sideband in the FMO protein as a critically damped quantum Brownian oscillator (time domain lineshape function g(t) given by Eq. 13 of ref. ⁴) with a frequency of $\omega/2\pi c = 70 \text{ cm}^{-1}$ and a stabilization energy of $\lambda/2\pi c = 30 \text{ cm}^{-1}$. As explained in the text, this reorganization energy has been used in a number of spectroscopic simulations⁵ because it effectively includes line broadening from both environmental motions and underdamped intramolecular vibrations with frequencies below 500 cm⁻¹; however, this reorganization energy significantly overestimates the FMO antenna's Stokes' shift at a temperature of 5K. Some fraction of the environmental reorganization energy and half of the intramolecular vibrational reorganization energy is anti-correlated, ⁷ so incorporation of these fractions of the total line broadening by convolution is an approximation. Code for evaluating the critically damped quantum oscillator's time domain lineshape function can be found in the EPAPS for ref. 8. The broadened absorption and emission cross-sections are obtained by convoluting the Brownian oscillator lineshape (given by Eqn. A3 in ref. 9) with the transition dipole strengths.

$$\sigma_{abs}(\omega) \simeq \operatorname{Re}\left[\int_{0}^{\infty} \left(\sum_{n,0,\nu_{A},\nu_{B}} \omega p_{0\nu_{A}\nu_{B}} \mid \mu_{n,0\nu_{A}\nu_{B}} \mid^{2} \exp[-i\omega_{n,0\nu_{A}\nu_{B}}t] \exp[-g(t)]\right) \exp(i\omega t) dt\right],$$

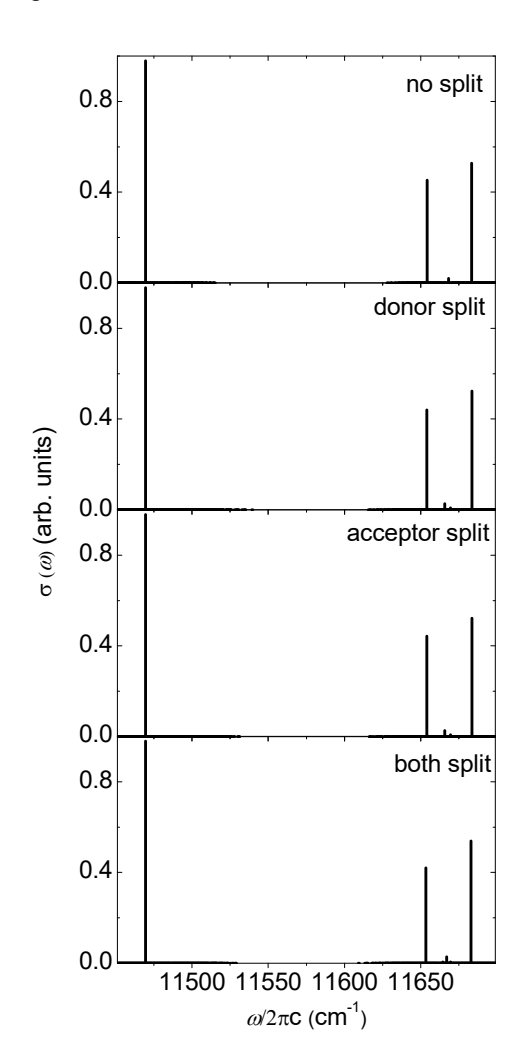
$$\sigma_{em}(\omega) \simeq \operatorname{Re}\left[\int_{0}^{\infty} \left(\sum_{n,0,\nu_{A},\nu_{B}} \omega p_{n} \mid \mu_{n,0\nu_{A}\nu_{B}} \mid^{2} \exp[-i\omega_{n,0\nu_{A}\nu_{B}}t] \exp[-g^{*}(t)]\right) \exp(i\omega t) dt\right].$$
(SM10)

S5. Effect of a Vibrational Splitting on either Donor or Acceptor

Figure S1 shows the effect of equally splitting the reorganization energy for the intramolecular vibration on either donor or acceptor over two modes. The stick spectra were calculated using the following parameters for the Hamiltonian in Eq. (1) of the main text for all 4 panels: $[(E^A + E^B)/2]/2\pi c = 11,574 \text{ cm}^{-1}; d_1^B = 0; \omega_2/2\pi c = 200 \text{ cm}^{-1}, d_2^A = 0; \omega_3/2\pi c = 200 \text{ cm}^{-1}, d_3^A = 0; \omega_3/2\pi c = 200 \text{ cm}^{-1}, d_3^$ 195 cm-1, $d_3^B = 0$; and $\omega_4 / 2\pi c = 195$ cm⁻¹, $d_4^A = 0$. Panel a (top) unequal frequencies, no vibrational splitting: $\omega_1 / 2\pi c = 197.5 \text{ cm}^{-1}$, $d_1^A \approx 0.225 (\lambda / 2\pi c = 5 \text{ cm}^{-1})$; $d_2^A = 0$ $d_2^B \approx 0.224 (\lambda / 2\pi c = 5 \text{ cm}^{-1})$ $\lambda/2\pi c$ 5 cm⁻¹), $d_3^A = d_4^B = 0$. Panel b) vibrational splitting of the donor pigment B: $\omega_1/2\pi c$ = 200 cm⁻¹, $d_1^A \approx 0.224$ ($\lambda/2\pi c = 5$ cm⁻¹), $d_2^B \approx 0.158$ ($\lambda/2\pi c = 2.5$ cm⁻¹), $d_3^A = 0$, $d_4^B \approx 0.24$ $0.160 \ (\lambda/2\pi c = 2.5 \ \text{cm}^{-1})$. Panel c) vibrational splitting of the acceptor pigment A: $\omega_1/2\pi c$ = 200 cm⁻¹, $d_1^A \approx 0.158 (\lambda / 2\pi c = 2.5 \text{ cm}^{-1}), d_2^B \approx 0.224 (\lambda / 2\pi c = 5 \text{ cm}^{-1}), d_3^A \approx 0.160 (\lambda / 2\pi c = 5 \text{ cm}^{-1})$ $\lambda/2\pi c$ 2.5 = cm⁻¹), $d_4^B = 0$. Panel d (bottom) vibrational splitting of both pigments: $\omega_1/2\pi c$ = 200 cm⁻¹, $d_1^A \approx 0.158 \ (\lambda/2\pi c = 2.5 \text{ cm}^{-1}), d_2^B \approx 0.158 \ (\lambda/2\pi c = 2.5 \text{ cm}^{-1}), d_3^A \approx 0.160 \ (\lambda/2\pi c = 2.5 \text{ cm}^{-1})$ $\lambda/2\pi c$ 2.5 = cm⁻¹), $d_4^B \approx 0.160$ ($\lambda/2\pi c$ 2.5 = cm⁻¹). The spectrum in panel d (frequencies of 200 and 195 cm⁻¹) differs very slightly from a spectrum with frequencies of 199 and 195 cm⁻¹ in Figure 5. The approximate displacements given are determined from the reorganization energies and vibrational frequencies through $\lambda = (1/2)\omega d^2$.

The acceptor splitting used here is symmetric and a crude approximation to that which might arise from a bilinear coupling between the excitonically resonant intramolecular vibration and a localized vibration of the acceptor environment (comparing panels a and c, the acceptor reorganization energy is symmetrically redistributed from an intramolecular vibration at 197.5 cm⁻¹ into two acceptor/environment modes at 195 cm⁻¹ and 200 cm⁻¹). The bilinear coupling model is commonly used to model vibrational relaxation into a continuum of bath states. The effects of an environmentally induced vibrational splitting on either donor or acceptor alone are both similar to the effects of intramolecularly induced vibrational splitting on both donor and acceptor in Figure 5 of the main text. In the spectrum, a single dominant vibronically resonant partner is reassembled by the vibrational excitonic resonance so that the spectrum is dominated by a single vibronic resonance splitting (peaks 2a and 2b). Small environmental splittings of either the donor or acceptor vibration do not appreciably disrupt the vibrational delocalization generated by vibrational-excitonic resonance.

Figure S1



References

- ¹ D. Papousek, and M. R. Aliev, *Molecular Vibrational-Rotational Spectra* (Elsevier Scientific, New York, 1982),
- ² R. C. Hilborn, Am. J. Phys. **50**, 982 (1982); R. C. Hilborn, Am. J. Phys. **51**, 471 (1983).
- ³ D. A. Farrow, W. Qian, E. R. Smith, A. A. Ferro, and D. M. Jonas, J. Chem. Phys. **128**, 144510 (2008); K. A. Kitney-Hayes, A. W. Albrecht-Ferro, V. Tiwari, and D. M. Jonas, J. Chem. Phys. **140**, 124312 (2014).
- ⁴ Y. Gu, A. Widom, and P. M. Champion, J. Chem. Phys. **100**, 2547 (1994).
- ⁵ Y.-C. Cheng, and G. R. Fleming, Annu. Rev. Phys. Chem. **60**, 241 (2009); Y. Fujihashi, G. R. Fleming, and A. Ishizaki, The Journal of Chemical Physics **142**, 212403 (2015).
- ⁶ A. Kell, K. Acharya, R. E. Blankenship, and R. Jankowiak, Photosynth. Res. **120,** 323 (2014).
- ⁷ V. Tiwari, W. K. Peters, and D. M. Jonas, J. Chem. Phys. **147**, 154308 (2017).
- ⁸ D. A. Farrow, A. Yu, and D. M. Jonas, J. Chem. Phys. **118**, 9348 (2003).
- ⁹ S. M. Gallagher Faeder, and D. M. Jonas, Phys. Rev. A **62**, 033820 (2000).